PL-TR-91-2157
Environmental Research Papers, No.1086

# IBSS Earth Backgrounds Experiment



R. A. Van Tassel,
Contributing Editor

24 June 1991



## Quick-Look Report





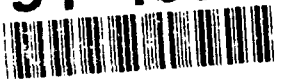

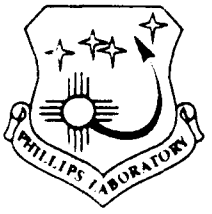


GEOPHYSICS DIRECTORATE OF
PHILLIPS LABORATORY
AIR FORCE SYSTEMS COMMAND
HANSCOM AIR FORCE BASE, MA 01731

"This technical report has been reviewed and is approved for publication"

WILLIAM A.M. BLUMBERG
Branch Chief

R. EARL GOOD
Division Director

This report has been reviewed by the ESD Public Affairs Office (PA) and is releasable to the National Technical Information Service (NTIS).

Qualified requestors may obtain additional copies from the Defense Technical Information Center. All others should apply to the National Technical Information Service.

If your address has changed, or if you wish to be removed from the mailing list, or if the addressee is no longer employed by your organization, please notify PL/IMA, Hanscom AFB, MA 01731-5000. This will assist us in maintaining a current mailing list.

Do not return copies of this report unless contractual obligations or notices on a specific document requires that it be returned.

# REPORT DOCUMENTATION PAGE

*Form Approved*
*OMB No. 0704-0188*



| 1. AGENCY USE ONLY (Leave blank) | 2. REPORT DATE | 3. REPORT TYPE AND DATES COVERED |
|---|---|---|
| | 24 June 1991 | Scientific, Interim |

**4. TITLE AND SUBTITLE**
IBSS Earth Backgrounds Experiment Quick-Look Report

**5. FUNDING NUMBERS**
PE 63220C
S3214201

**6. AUTHOR(S)**
Roger A. Van Tassel, Contributing Editor

**7. PERFORMING ORGANIZATION NAME(S) AND ADDRESS(ES)**
Phillips Laboratory (OPB)
Geophysics Directorate
Optical Environment Division
Hanscom AFB, MA 01731

**8. PERFORMING ORGANIZATION REPORT NUMBER**
PL-TR-91-2157
ERP, No. 1086

**9. SPONSORING/MONITORING AGENCY NAME(S) AND ADDRESS(ES)**
SDIO/TNS
The Pentagon
Washington, DC 20301

**10. SPONSORING/MONITORING AGENCY REPORT NUMBER**

**11. SUPPLEMENTARY NOTES**

**12a. DISTRIBUTION/AVAILABILITY STATEMENT**
Approved for public release; distribution unlimited

**12b. DISTRIBUTION CODE**

**13. ABSTRACT (Maximum 200 words)**

The Infrared Background Signature Survey (IBSS) was a Strategic Defense Initiative Organization (SDIO)-sponsored and managed experiment designed to collect infrared, ultraviolet, and visible data for use in the development of Ballistic Missile Defense Sensor Systems. The IBSS backgrounds experiment was designed to acquire SWIR and MWIR data in the low earthlimb and against the hard earth. The infrared sensors were located on a Shuttle Pallet Satellite (SPAS) which was berthed in the orbiter until its deployment for measurements. The Shuttle Discovery, STS-39, was launched on April 28, 1991 at 0733 from Kennedy Space Center. Twenty -two measurement blocks were made. These included measurements of the solar specular region, hard earth, earthlimb, and aurora. This report is a Quick-Look at the earth background results using the real-time 8 Kbit telemetry stream.

| 14. SUBJECT TERMS | 15. NUMBER OF PAGES |
|---|---|
| Infrared, Earth Backgrounds | 56 |
| | 16. PRICE CODE |

| 17. SECURITY CLASSIFICATION OF REPORT | 18. SECURITY CLASSIFICATION OF THIS PAGE | 19. SECURITY CLASSIFICATION OF ABSTRACT | 20. LIMITATION OF ABSTRACT |
|---|---|---|---|
| Unclassified | Unclassified | | UL |

# Executive Summary

*by Roger A. Van Tassel*

The Infrared Background Signature Survey (IBSS) was a Strategic Defense Initiative Organization (SDIO)-sponsored and managed experiment designed to collect infrared, ultraviolet, and visible data for use in the development of ballistic missile defense sensor systems. The President has directed that the SDI program be refocused with the principal objective of providing protection from limited ballistic missile strikes, whatever their source. The acronym for this new revised approach is GPALS, which stands for Global Protection Against Limited Strikes. It represents an important change and will require systems with much shorter response times, with the ability to acquire and track targets against low altitude regions of the earth's atmosphere or against the hard earth. The IBSS backgrounds experiment was designed to acquire data in this altitude region, primarily in the mid-wave infrared at 4.3 μm. The infrared sensors were located on a Shuttle Pallet Satellite (SPAS) which was berthed in the orbiter until its deployment for measurements. The prime contractor for the program is Messerschmitt-Bolkow-Blohm (MBB) of Germany.

The shuttle Discovery, STS-39, was launched on 28 April, 1991 at 0733:13.98 Eastern Daylight Time (GMT: 118:11:33:14) from Kennedy Space Center. The Discovery cargo consisted primarily of AFP-675 and IBSS. Approximately 41 minutes after launch the orbiter was inserted into a near circular orbit of approximately 138 nautical miles with an inclination of approximately 57°. The SPAS was deployed from the orbiter at mission elapsed time (MET) 2 days, 20 hours, 44 minutes (orbiter revolution 47).

During the SPAS deployed and RMS operations 22 measurement blocks were made of the solar specular region, hard earth, earthlimb, and aurora. All major backgrounds

experimental objectives were achieved. Extensive measurements were made of the $CO_2$ backgrounds in earthscan, and both horizontal and vertical earthlimb modes. Additional measurements were made throughout the SWIR and MWIR spectral regions (2.3 - 7.7 μm) in both the earthlimb and hard earth modes.

The most stressing region of the natural background is thought to be in the vicinity of the solar specular point. It is for this reason that the primary objective of the IBSS earth backgrounds experiment was measurement of the background structure in two $CO_2$ bands at 4.3 μm as the solar specular point was scanned. While the wide-band background was expected to show some structure, it was not expected to show the variations that were observed in this experiment. Because the narrow band receives radiation from the center of the $CO_2$ absorption band, where the atmosphere is both cold and well mixed, it was expected that any structure in this band would be below the sensitivity of the radiometer. The results show that this is not the case, as significant structure is also observed in this narrow band.

It must be emphasized that these data are extremely preliminary. The real-time data stream consists of only the inphase value of the detector output, at only 1/20 of the recorded rate. While the footprint of the detectors is less than 100 meters, the real-time data only samples every 2 kilometers.


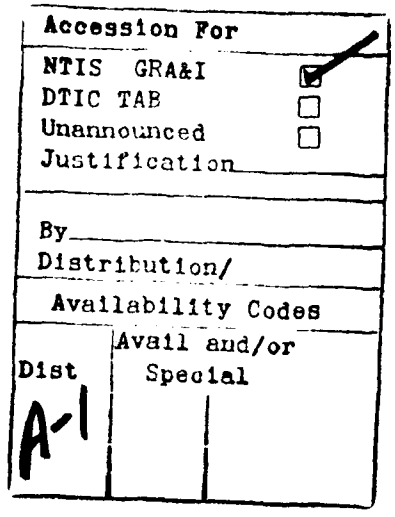


# Contents

# Illustrations

## Tables

# Acknowledgements

An experiment of this magnitude is not possible without the cooperation and hard work of a large number of people. It is not possible to acknowledge here all of the people who contributed to this very successful mission, but the author does wish to acknowledge those who made direct contributions to this report. In particular, I wish to thank William Grieder of Grieder Research Engineering, and Cynthia Beeler of Visidyne for the engineering analysis of the IBSS infrared sensors, and for operating a "backroom" environment on site during the mission which provided much of the input for this report. I also wish to acknowledge the significant contribution of Dr. Charles Humphrey, also of Visidyne, for backup and support in the Payload Operations Control Center. Karen Kennedy of SKW, Inc., and Gerald Lamb and David Monteiro of Nichols Research Inc. provided real-time data on disks for rapid analysis during the mission: Capt. Deanna Ramirez of the USAF/Air Weather Service provided maps of the world showing cloud cover and structure; Greg Picard of Barrios Inc. provided maps of our line-of-sight during the mission, and Guenter Lange of Messerschmitt-Bolkow-Blohm provided preliminary instrument performance, again, in real time during the mission. I also wish to thank the IBSS Program Manager, Michael E. Harrison of SDIO, for his active involvement and enthusiastic support throughout the program.

# IBSS Earth Backgrounds Experiment

## 1. INTRODUCTION

*by Roger A. Van Tassel, William F. Grieder, Cynthia J. Beeler, and Charles H. Humphrey*

The Infrared Background Signature Survey (IBSS) was a Strategic Defense Initiative Organization (SDIO)-sponsored and managed experiment designed to collect infrared, ultraviolet, and visible data for use in the development of ballistic missile defense sensor systems. The President has directed that the SDI program be refocused with the principal objective of providing protection from limited ballistic missile strikes, whatever their source. The acronym for this new revised approach is GPALS, which stands for Global Protection Against Limited Strikes. It represents an important change and will require systems with much shorter response times. It will also require systems that have the ability to acquire and track targets against low altitude regions of the earth's atmosphere or against the hard earth. The IBSS backgrounds experiment was designed to acquire data in this altitude region, primarily in the mid-wave infrared at 4.3 μm. The infrared sensors were located on a Shuttle Pallet Satellite (SPAS) (see Figure 1) which was berthed in the orbiter until its deployment for measurements. The prime contractor for the program is Messerschmitt-Bolkow-Blohm (MBB) of Germany.

The infrared instruments on IBSS were supplied by MBB and consisted of a 29-detector radiometer and a 12-detector infrared Ebert-Fastie type grating spectrometer. The nominal

(Received for Publication 21 June 1991)

radiometer and spectrometer focal plane dimensions and layouts in object space are shown in Figure 2. These instruments were mated with a high-off-axis-rejection telescope. Both the sensors and the telescope were cooled within a liquid helium cryostat. The radiometer spectral range covered the region from 2.4 to 8 μm by selecting one of seven optical filters. Some bands were provided with neutral density filters to reduce the responsivity for measurements of plume radiances. The relative spectral response for the filters in the radiometer are shown in Figure 3.

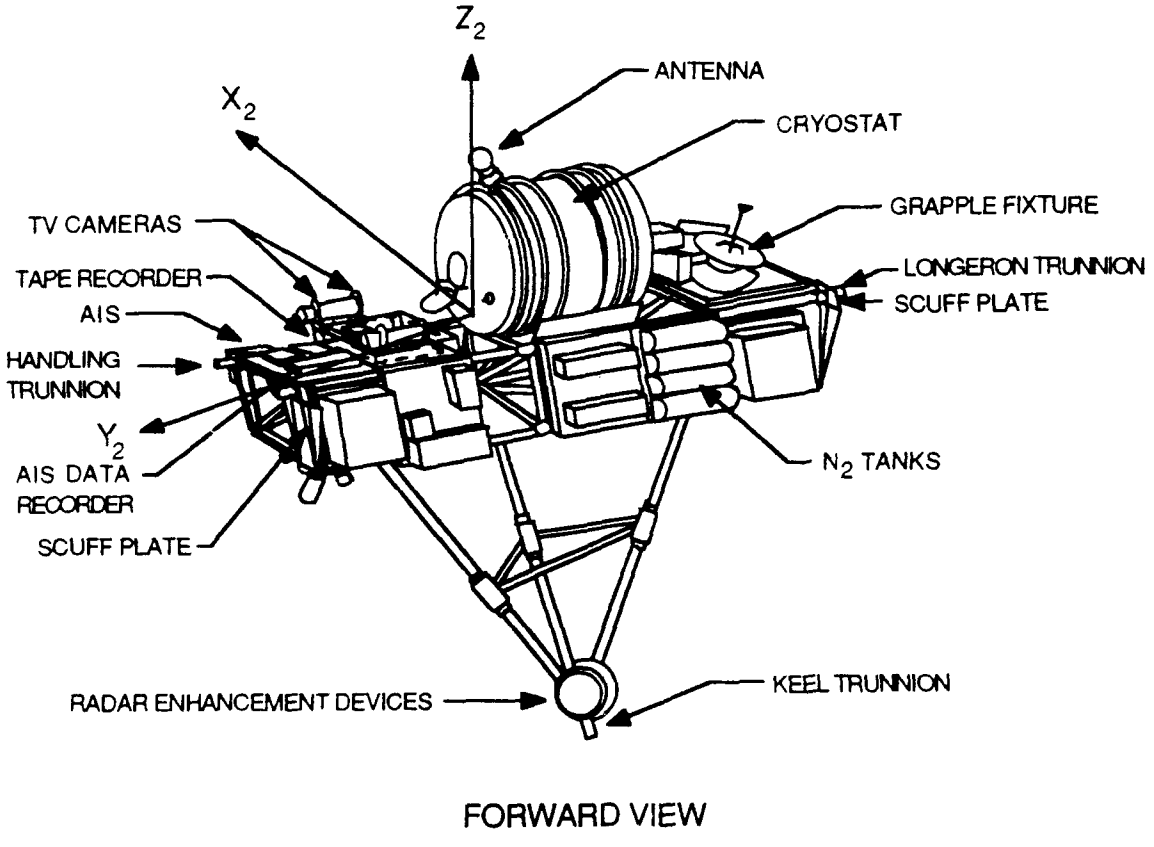


Figure 1. Drawing of the SPAS Spacecraft Showing the Cryostat Which Houses the IBSS Radiometer and Spectrometer.

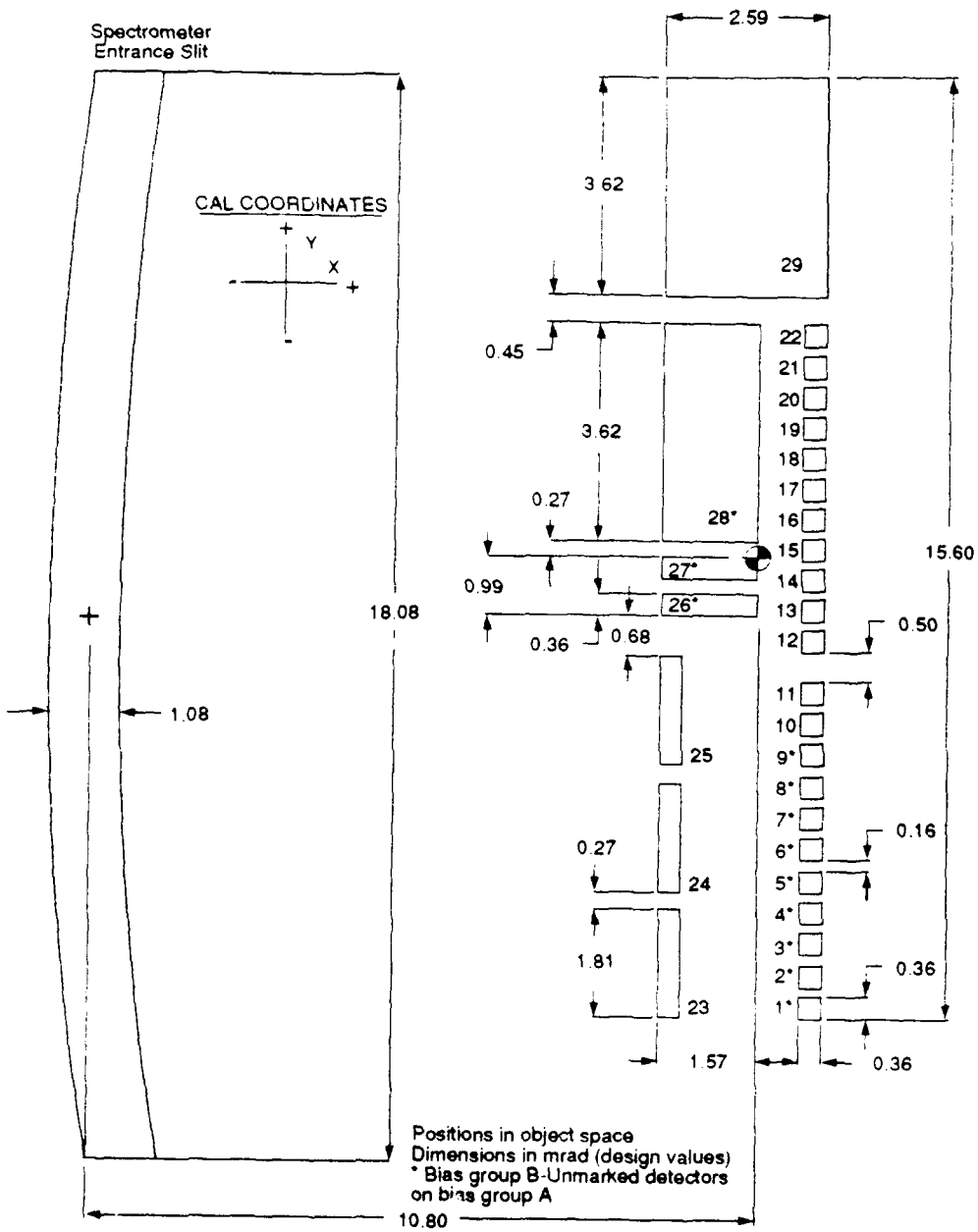


Figure 2. IBSS Radiometer and Spectrometer Focal Plane Numbering System and Layout in Object Space (from USU/SDL Calibration Report).

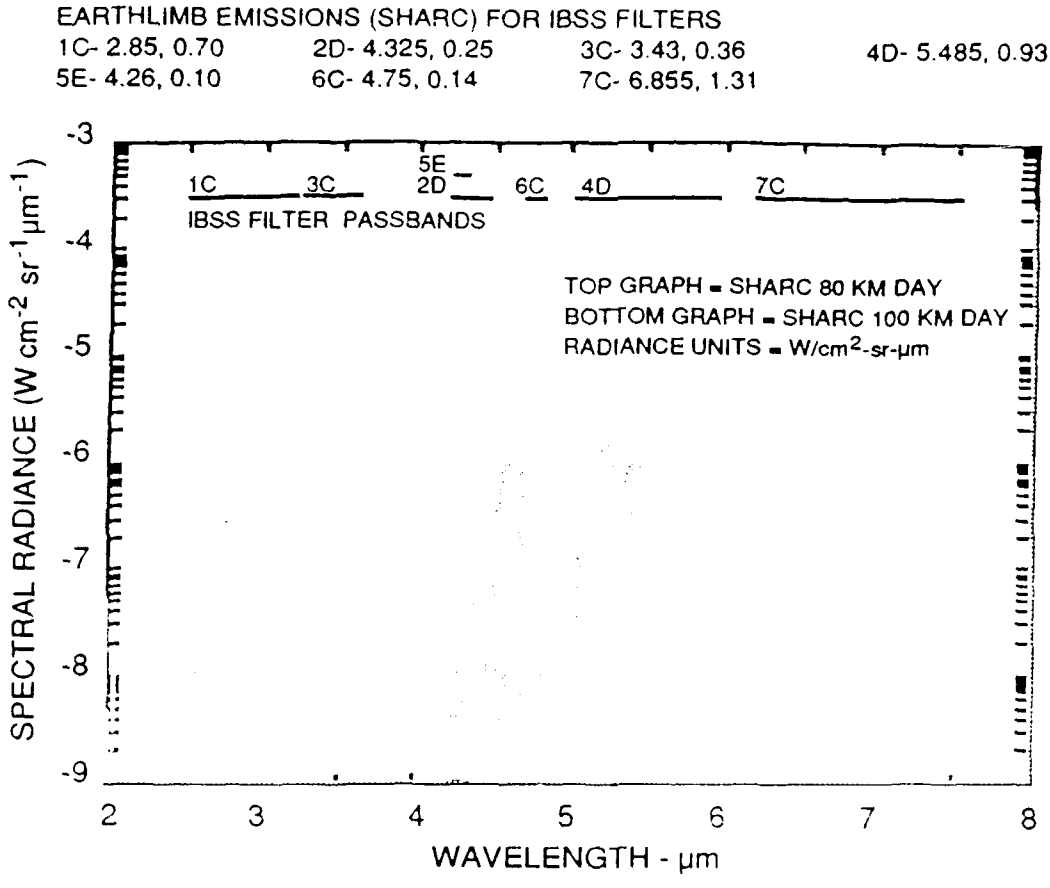


Figure 3. Earthlimb Infrared Emission Predictions (SHARC) for 80 and 100 km Tangent Height Showing the Spectral Coverage of the IBSS Infrared Sensor Filter Passband. See Table 1 for specie identification.

The shuttle Discovery, STS-39, was launched on 28 April, 1991 at 0733:13.98 Eastern Daylight Time (GMT: 118:11:33:14) from Kennedy Space Center. The Discovery cargo consisted primarily of AFP-675 and IBSS. Approximately 41 minutes after launch the orbiter was inserted into a near circular orbit of approximately 138 nautical miles with an inclination of approximately 57°. The SPAS was deployed from the orbiter at mission elapsed time (MET) 2 days, 20 hours, 44 minutes (orbiter revolution 47).

One of the primary objectives of the IBSS mission was to measure spatial clutter in emissions from both the earthlimb and the hard earth by scanning the earth using the orbital motion of the SPAS. Figures 3 and 4 show model predictions of the infrared emission intensities measured with the IBSS radiometer during these experiments. The spectral coverage of the IBSS filters is also indicated in the figures. It was expected that the radiance variation or clutter, associated with these emissions would be only a small percentage of the mean intensities given in these figures. Infrared emissions observed in the earthlimb have sources that are minor species of the atmosphere and which are excited by a variety of processes. Some of the known infrared emission sources are given in Table 1.

Table 1. Earthlimb Atmospheric Infrared Emissions

| Radiating Specie | Wavelength μm | Radiating Specie | Wavelength μm |
|---|---|---|---|
| NO first overtone | 2.7 | CO | 4.6 |
| OH fundamental | 2.7 | $O_3$ $\nu_1 + \nu_3$ comb. | 4.8 |
| $H_2O$ $\nu_1$ and $\nu_3$ | 2.7 | NO fundamental | 5.3 |
| $CH_4$ $\nu_3$ | 3.3 | $NO_2$ $\nu_3$ | 6.2 |
| $CO_2$ $\nu_3$ | 4.3 | $H_2O$ $\nu_2$ | 6.3 |
| $N_2O$ | 4.5 | $N_2O$ | 7.8 |

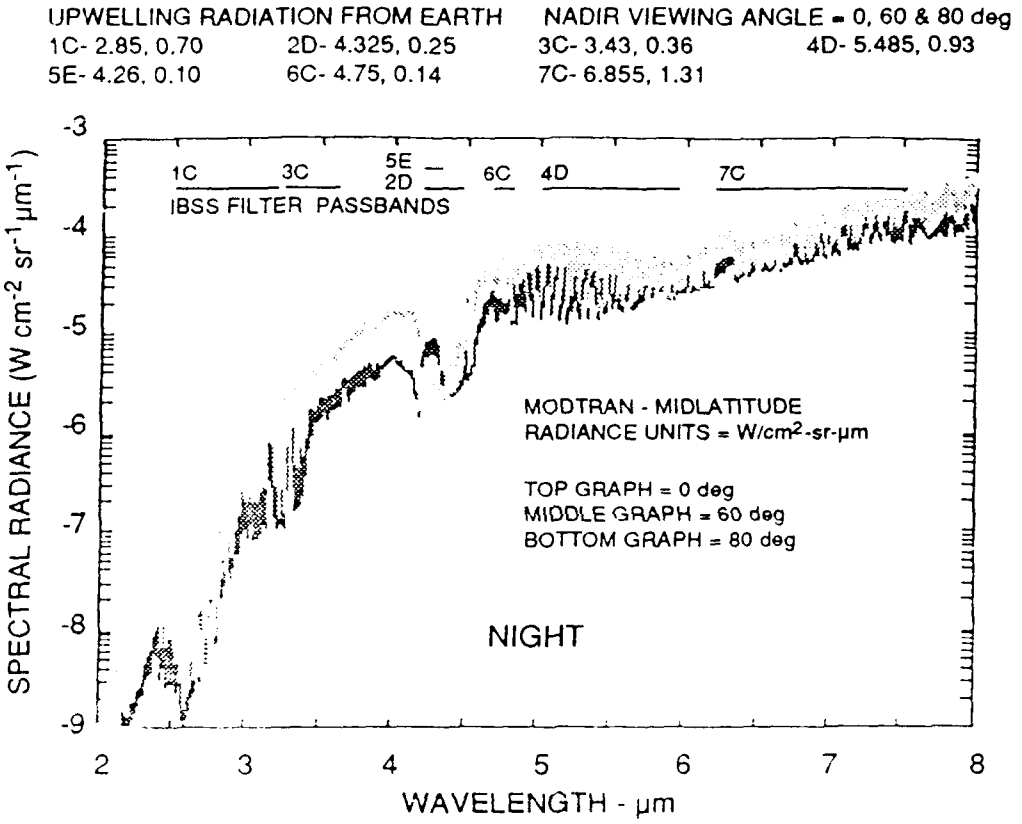


Figure 4. Predictions (MODTRAN) of Upwelling Infrared Radiation from the Hard Earth to Space at Nadir Viewing Angles of 0, 60, and 80 Degrees and Showing the Spectral Coverage of the IBSS Infrared Sensor Filter Passbands.

## 2. INSTRUMENTATION DESCRIPTION

*by William F. Grieder and Cynthia J. Beeler*

### 2.1 SPAS

This flight is the third flight of the German built SPAS, a Shuttle Pallet Satellite that is carried into orbit by the shuttle (see Figure 1). Measurements can be made from within the orbiter bay, from the end of the Canadian built remote manipulator system (RMS), or deployed in space. The SPAS structure carries the IBSS sensors and provides power, telemetry, and recording of both the housekeeping and science data. Nitrogen jets are used to control attitude and pointing. The pointing and attitude data in this report were generated by the on-board gyros and taken from the 8 kbit real-time telemetry stream.

### 2.2 Infrared Radiometer

A brief description is given here of the signal generation and flow in the IBSS radiometer sensor. More detailed information on the signal processing can be found in the IBSS Critical Design Review (CDR).

A simplified component diagram of the front end section of the IBSS radiometer system is shown in Figure 5. The source radiation is collected by the telescope and transferred off of secondary mirrors in the telescope to the optical filter wheel assembly, which consists of calibration devices and interference filters. The relative spectral response of the filters is shown in Figure 6. The analysis of the telescope and the optical filters has been documented previously by Grieder, Beeler, and Wilson*, and will not be considered further in this report.

After the filters, the radiation is chopped by a tuning fork optical chopper (operating at approximately 238 Hz) and is imaged to 29 indium doped silicon detectors (Si:In) which are cryogenically cooled (nominally 14.5 K ). The signal generated in the detectors is a chopped waveform modulated by the source radiation. Each detector has its own amplifier. The detector output is coupled to a transimpedance amplifier (TIA) consisting of a metal oxide semiconductor field effect transistor (MOSFET) and an operational amplifier. A critical section of the TIA is the feedback network which contains a $3 \times 10^9$ ohm resistor and an effective distributed capacitance of 0.3 pF (estimate). The TIA circuitry is compensated so that the frequency response is better than what would be calculated from the feedback resistor and the distributed capacitance.

* Grieder, W. F., Beeler, C.J., and Wilson, R. W. (1988). *IBSS Radiometer Optical Filter and Noise Analysis*. Utah State University, USU-88-526, Logan, UT.

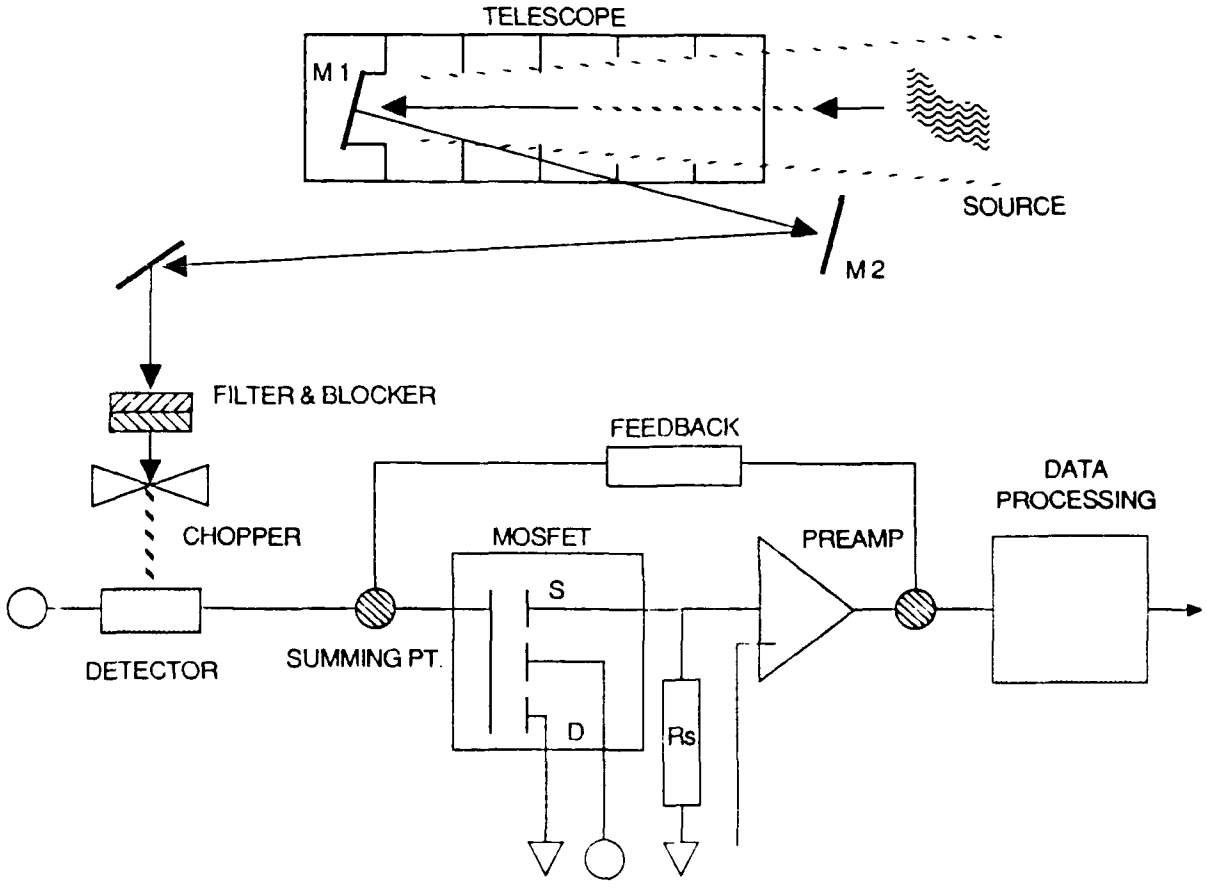


Figure 5. IBSS Radiometer Signal Flow Schematic Showing the Transimpedance Amplifier with its Feedback Circuit.

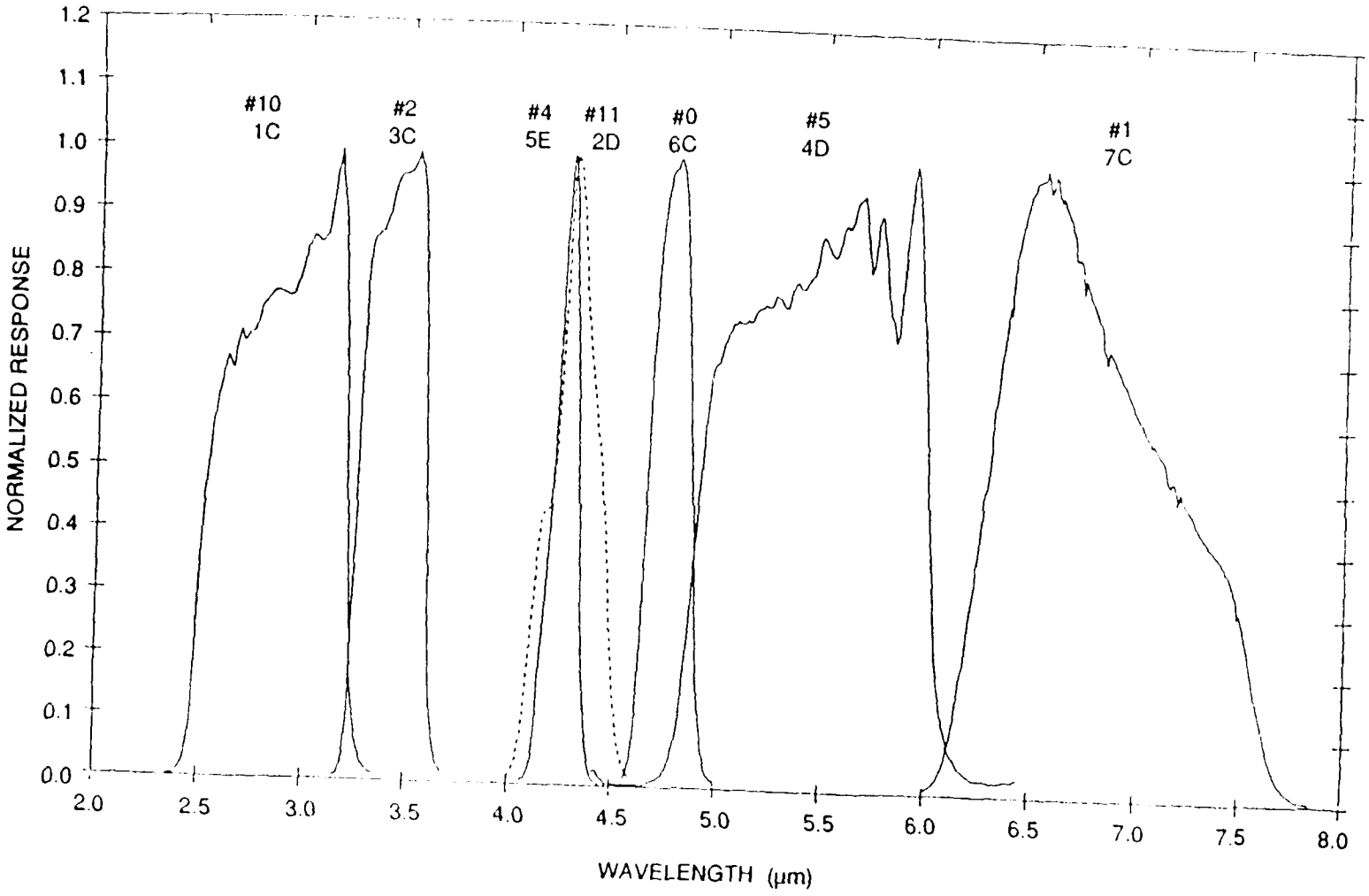


Figure 6. Relative Filter Response of the IBSS Radiometer Optical Filters. (From IBSS IR Sensor Calibration Final Report, L. Jacobson and S. Sargent, Space Dynamics Laboratory, Utah State University, 1 Jan. 90).

Following the TIA, the signal is filtered by an electronic bandpass filter with a 50 Hz bandpass centered at the chopping frequency. The bandpass filter removes the DC and all the signal harmonics except the fundamental. The signal is then amplified (×1, ×16 or ×256), sampled at six times the chopper frequency, digitized, and demodulated by multiplying by a cosine and sine function with arguments of the chopping frequency. This quadrature demodulation produces what are called the in-phase signal component or "I-value" and the quadrature component or "Q-value". This is the first step in demodulating the signal. The phase of the demodulating cos/sinusoids was pre-selected to maximize the I-value. Both the I- and Q-values are averaged over 18 samples (three cycles of the chopper), formatted, and recorded. In concept, the demodulated signal is considered to be equal to the square root of the sum of the squares of the I- and Q-values after DC offsets are removed. However, for the real-time 8 kbit telemetry data presented here, only the I-values were transmitted. The phase for each detector was established pre-flight using engineering test data. The radiances estimated in this report were derived by dividing the I-values by the cosine of the assumed phase angle.

There are 32 output data channels, one for each of the 29 detectors as well as 3 additional amplified (fixed gain) signals from detectors 27, 28, and 29, designated 27A, 28A, and 29A respectively. The signal amplification is accounted for in the onboard data processing except for channels 27A, 28A, and 29A.

The angular and physical dimensions for each radiometer detector are given in Table 2.

Table 2. IBSS Radiometer Detector Parameters

| Detector Numbers | Angular Dimensions milliradians | Physical Dimensions µm |
|---|---|---|
| 1 through 22 | 0.36 × 0.36 | 200 × 200 |
| 23 through 25 | 0.36 × 1.81 | 200 × 1000 |
| 26 & 27 | 0.36 × 1.57 | 870 × 200 |
| 28 | 1.57 × 3.62 | 870 × 2000 |
| 29 | 2.69 × 3.62 | 1485 × 2000 |

## 2.3 Spectrometer

The IBSS spectrometer is a 12-detector Ebert-Fastie type with a single collimating mirror between the entrance and exit slits. Six cryogenically cooled (Si:Bi and Si:As) detectors cover 5 grating orders from 2.5 to 24 µm (See Table 3.) The approximate resolution is 1/300. The second set of 6 ectors is redundant and covers the identical wavelength regions. The system shares the radiometer telescope and contains its own tuning fork optical chopper with a chopping frequency of approximately 240 Hz. The detector temperature is of the order of

14.5 K. The signal processing in the spectrometer was similar to that of the radiometer except that 12 samples were averaged to obtain the I- and Q-values. The radiometer and spectrometer data could not be recorded simultaneously.

Table 3. IBSS Spectrometer Wavelength Coverage

| Channel | Grating Order | Wavelength-μm | Estimated NESR* |
|---|---|---|---|
| 1 | 5 | 2.5 - 3.2 | 3E-4 |
| 2 | 4 | 3.4 - 4.0 | 2E-4 |
| 3 | 3 | 4.2 - 5.6 | 9E-5 |
| 4 | 2 | 5.6 - 8.4 | 5E-5 |
| 5 | 1 | 8.4 - 17 | 2E-5 |
| 6 | 1 | 17 - 24 | 1.5E-5 |

* Watts/cm$^2$-sr-μm - based on viewing the hard earth (from Matson, SKW)

## 3. FLIGHT SUMMARY AND SENSOR PERFORMANCE

*by William F. Grieder and Cynthia J. Beeler*

### 3.1 Shuttle Launch and Flight Description

Discovery, STS-39, was scheduled for launch on 23 April, 1991 but in the early morning hours of the launch day a malfunctioning transducer was discovered in the orbiter. The countdown was aborted. The launch was rescheduled for 28 April, 1991 at 0701 EDT after NASA replaced the transducer.

At T-9 minutes on launch day a hold was implemented because an operational tape recorder started without a command. This malfunction was resolved and the shuttle Discovery, STS-39, lifted off on 28 April, 1991 at 0733:13.98 Eastern Daylight Time (EDT) from Kennedy Space Center. Approximately 41 minutes after launch the orbiter was inserted into a near circular orbit of approximately 138 nautical miles with an inclination of approximately 57°.

### 3.2 SPAS Performance Summary

On 29 April a decision was made to delay the deployment of SPAS and the IBSS experiment for 24 hours to permit CIRRIS 1A, an experiment on the AFP-675 payload, to complete their experiments before running out of cryogen. The SPAS was powered up on MET day 2 and all in-bay checks were performed satisfactorily. SPAS was deployed from the orbiter at MET 2 days, 20 hours, 44 minutes (orbiter revolution 47). During SPAS attitude alignment (strapdown) the sun sensor apparently locked onto a false source, suspected to be the reflection of the sun from an orbiter wing. This corrupted the alignment procedure. The error was corrected at approximately MET 3 days, 5 hours, 40 minutes. As a result of the delay, Measurement Set 2 was rescheduled for a later time. Preliminary as-flown ephemerides for the SPAS during the background experiments are given in Appendix B.

In general the SPAS performed well and first indications are that the pointing was accurate and stable.

### 3.3 Radiometer Performance

On GMT day 118 the IBSS IR radiometer was powered up while still berthed in the shuttle bay. Telemetry data was recorded while the sensor viewed internal calibration sources. The focal plane temperature during these tests remained stable at 14.35 K. Several measurements were made using filter position 3 with the internal calibration source off. These data provided a means to check detector operation status, I-value dark offsets, and dark noise. A sample of these data is shown in Figure 7 and a summary is given in Table 4. Offsets are given in I-value

counts. The noise was derived from the time series variance using the conversion 1.2E8 counts per volt with a bandwidth of approximately 2 Hz.

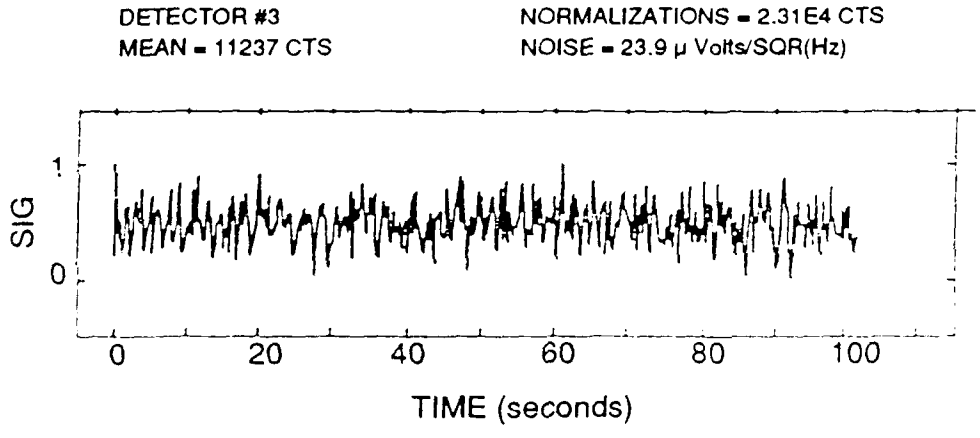


Figure 7. Sample I-Data from Radiometer Closed Cover Test from First Infrared Sensor Power Up.

Table 4. Sample of Close Cover Test of IBSS Radiometer

| DET | I-offsets* | Noise** |
|---|---|---|
| 1 | 3886 | 1.1636 E-5 |
| 2 | 3630 | 1.06433 E-5 |
| 3 | 11237 | 2.38963 E-5 |
| 4 | 3507 | 1.01311 E-5 |
| 5 | 3848 | 1.14526 E-5 |
| 6 | 3474 | 1.00931 E-5 |
| 7 | 4579 | 1.29018 E-5 |
| 9 | 3788 | 1.287 E-5 |
| 10 | 3674 | 1.0212 E-5 |
| 11 | 4435 | 1.10689 E-5 |
| 12 | 7465 | 1.16759 E-5 |
| 13 | 6449 | 1.20722 E-5 |
| 14 | 5015 | 1.1587 E-5 |
| 15 | 4197 | 1.12761 E-5 |
| 16 | 3973 | 1.11958 E-5 |
| 17 | 5308 | 1.12492 E-5 |
| 18 | 5622 | 1.35634 E-5 |
| 19 | 4743 | 1.17355 E-5 |
| 20 | 4929 | 1.58974 E-5 |
| 21 | 10217 | 4.3813 E-5 |
| 22 | 86112 | 3.80199 E-4 |
| 23 | 1458 | 6.28255 E-6 |
| 24 | 1099 | 5.08607 E-6 |
| 25 | 1415 | 6.10295 E-6 |
| 26 | 5669 | 1.09253 E-5 |
| 27 | 4701 | 1.06171 E-5 |
| 28 | 919 | 3.82712 E-6 |
| 29 | 5848 | 1.24429 E-5 |
| 30 | 158 | 1.0606 E-6 |
| 31 | 18989 | 2.69252 E-4 |
| 32 | 251 | 3.7003 E-6 |

* Units - Counts

** Units - μV/Hz 1/2

### 3.4 8 Kbit Telemetry

Data from the 8 kilobit real-time telemetry was read by the operational team at the Payload Operations Control Center (POCC), reformatted into packed files, and recorded on floppy disks. These disks were transferred to the principal investigator (PI) team for evaluation. The disks were unpacked into the 39 channels of IBSS data shown in Table 5. This data consisted of 32 channels of science and housekeeping data as indicated. The sampling rate for these data was 4 Hz and consists of the I-values only. The Q-values are not available on the 8 kilobit channel.

In addition to the IR sensor data, SPAS attitude data was also telemetered. These data provided the SPAS yaw, pitch and roll Euler angles versus time. The data were listed in columns as roll, pitch and yaw even though the Euler sequence was yaw, pitch, and roll. They were sampled at 1 Hz.

Table 5. 8 Bit Telemetry Assignments

| Channel | Parameter |
|---|---|
| 1 | index |
| 2 - 33 | radiometer I-values |
| 34 | filter position |
| 35 | scan mirror angle |
| 36 | grating mirror angle |
| 37 | overflow bit |
| 38 | mode |
| 39 | elapsed time |

### 3.5 Radiometer Data Reduction

Reduction of the radiometer sensor data was performed using the telemetry data indicated above and calibration data obtained from the USU calibration report. One of the first tasks was to determine the dc offsets for the I-values from the closed cover flight data. This was done by finding the average value of the I-signals for each closed cover measurement and averaging the group. The results are listed in Table 6 along with phase angles determined preflight from engineering test data.

Table 6. Radiometer Channel dc Offsets and Phase

| Channel | Offset (cts) | Phase (deg) | Channel | Offset (cts) | Phase (deg) |
|---|---|---|---|---|---|
| 1 | 3886 | -4.25 | 17 | 5308 | -5.0 |
| 2 | 3630 | -8.73 | 18 | 5622 | -7.26 |
| 3 | 11237 | -9.58 | 19 | 4743 | -1.07 |
| 4 | 3507 | -6.72 | 20 | 4929 | -5.70 |
| 5 | 3848 | -8.46 | 21 | 10217 | -6.48 |
| 6 | 3474 | +0.095 | 22 | 86112 | -5.66 |
| 7 | 4579 | -6.78 | 23 | 1458 | -7.69 |
| 8 | 3703 | -6.52 | 24 | 1099 | -8.07 |
| 9 | 3788 | -5.54 | 25 | 1415 | -8.07 |
| 10 | 3674 | -5.39 | 26 | 5669 | -6.09 |
| 11 | 4435 | -8.29 | 27 | 4701 | -2.64 |
| 12 | 7465 | -9.49 | 28 | 919 | -5.34 |
| 13 | 6449 | -6.60 | 29 | 5845 | -4.93 |
| 14 | 5015 | -5.79 | 30 | 158 | -2.94 |
| 15 | 4197 | -3.20 | 31 | 18989 | +6.11 |
| 16 | 3973 | -2.15 | 32 | 251 | +2.59 |

The radiance L(D) for each detector D was computed using

$$L(D) = \frac{C(F.D)\,[I(D) - Io(D)]}{\cos\theta(D)} \quad \text{Watts/sq cm-sr}$$

where

C(F.D) = inverse responsivity for detector D and filter F - Watts/sq cm-sr/counts

I(D) = I-signal for detector D from TM - counts

Io(D) = DC or dark offset for detector D - counts

$\theta(D)$ = phase angle for detector D = degrees

## 4. MEASUREMENT SUMMARY

*by Roger A. Van Tassel, Charles H. Humphrey, Cynthia J. Beeler and William F. Grieder*

A summary of the IBSS measurements is given in Table 7. The times are given in Mission Elapsed Time (MET). They may be converted to Universal Time (UT) by adding the launch time which is 118 days, 11 hours, 33 minutes, 14 sec.

Table 7. Summary of IBSS Earth Backgrounds Experiments

| Experiment Description | Start Time-MET dy:hr:min | End Time-MET dy:hr:min | Orbit | Comments |
|---|---|---|---|---|
| $CO_2$ Earthscan | 03:07:23 | 03:08:51 | 54/55 | |
| SSP/Spatial 2D | 03:12:08 | 03:12:22 | 57 | |
| Limb to Earth, ALL | 03:15:31 | 03:15:36 | 59 | Night |
| Limb to Earth, 2D | 03:15:55 | 03:15:57 | 59 | Night |
| Limb to Earth, 5E | 03:15:59 | 03:16:17 | 60 | Night |
| SSP/Spatial, 5E | 03:16:38 | 03:16:52 | 60 | |
| $CO_2$ Earthlimb | 04:00:45 | 04:02:15 | 65/66 | |
| SSP/Spatial, 5E R | 04:04:28 | 04:04:43 | 68 | |
| Measurement Set 2 | 04:05:10 | 04:05:57 | 68/69 | Horizontal limb scans |
| Limb to Earth, ALL | 04:06:10 | 04:06:27 | 69 | Day |
| SSP/Spatial, 7C | 04:08:57 | 04:09:10 | 71 | |
| MWIR Earthscan | 05:03:42 | 05:04:02 | 83/84 | Term |
| SSP/Spatial, 2D R | 05:04:21 | 05:04:36 | 84 | |
| NO Earthlimb | 05:05:04 | 05:05:07 | 84 | Night |
| Aurora | 05:05:33 | 05:05:42 | 84/85 | |
| SSP/Spectral | 05:09:00 | 05:09:20 | 87 | |
| NO Earthlimb | 05:13:55 | 05:14:10 | 90 | Night |
| Elmb, 7C, Term | 05:14:15 | 05:14:35 | 91 | 115 Km |
| Measurement Set 2R | 05:15:29 | 05:16:40 | 91/92 | |
| Elmb, 7C, Term | 05:18:40 | 05:18:57 | 94 | 30 Km |
| NO Earthlimb | 05:19:17 | 05:19:25 | 94 | Day |
| MWIR Earthscan | 05:20:00 | 05:21:00 | 95/96 | 7C Term |

### 4.1 $CO_2$ Earthscan

The $CO_2$ earthscan was the first earth backgrounds measurement. It was planned to scan the earth while manually sequencing between the two $CO_2$ filter bands. The measurement was started with filter 2D, and even though uplink commands were sent to move to filter 5E, the filter position did not change. This was reported and corrected within about fifteen minutes. It was found that the pre-stored ground command sequence was too fast to be recognized by the

filter positioning system. After a one second delay was inserted between uplink commands, the commands were recognized and the system operated normally throughout the remainder of the measurement. Lightning flashes were observed on the real time $L^3TV$ as the spacecraft passed over Japan. The spacecraft and field of view ground tracks are shown in Figure 8. Cloud patterns were provided by the DMSP imagery and are shown in Figure 9. The $CO_2$ earthscan was done in one extended observation period and covered day, night, and two terminators. The initial attitude angles (roll, pitch, and yaw) were -.05, -24.1, and -137.1 degrees respectively. A preliminary output of the entire $CO_2$ earthscan sequence was provided by MBB and is shown in Figure 10. Figures 11 and 12 show a sample of this data for the narrow band and wide-band respectively.

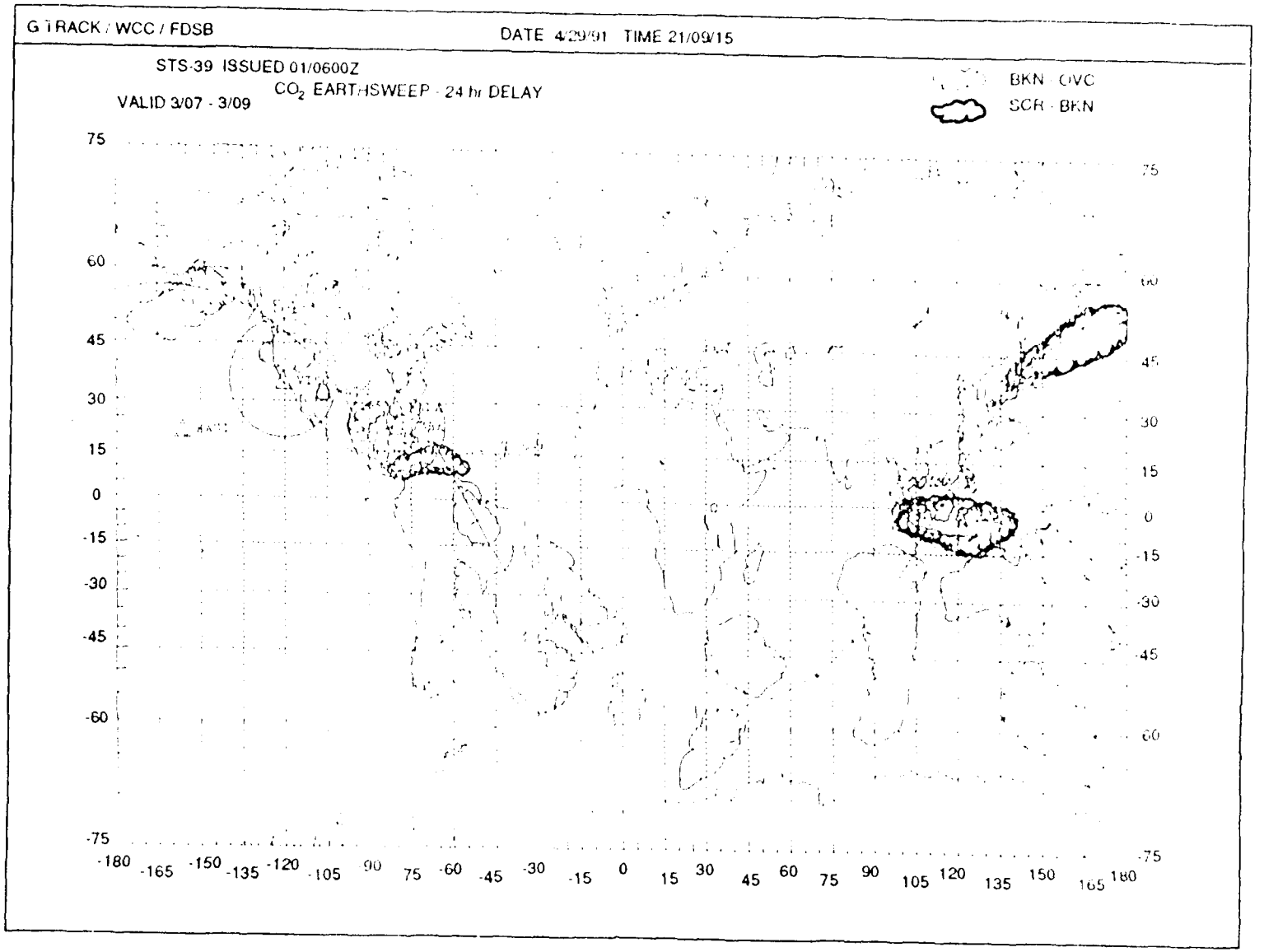


Figure 8. Orbit 54 Spacecraft and Field-of-View Ground Tracks.
Courtesy of Greg Picard, Barrios, Inc.

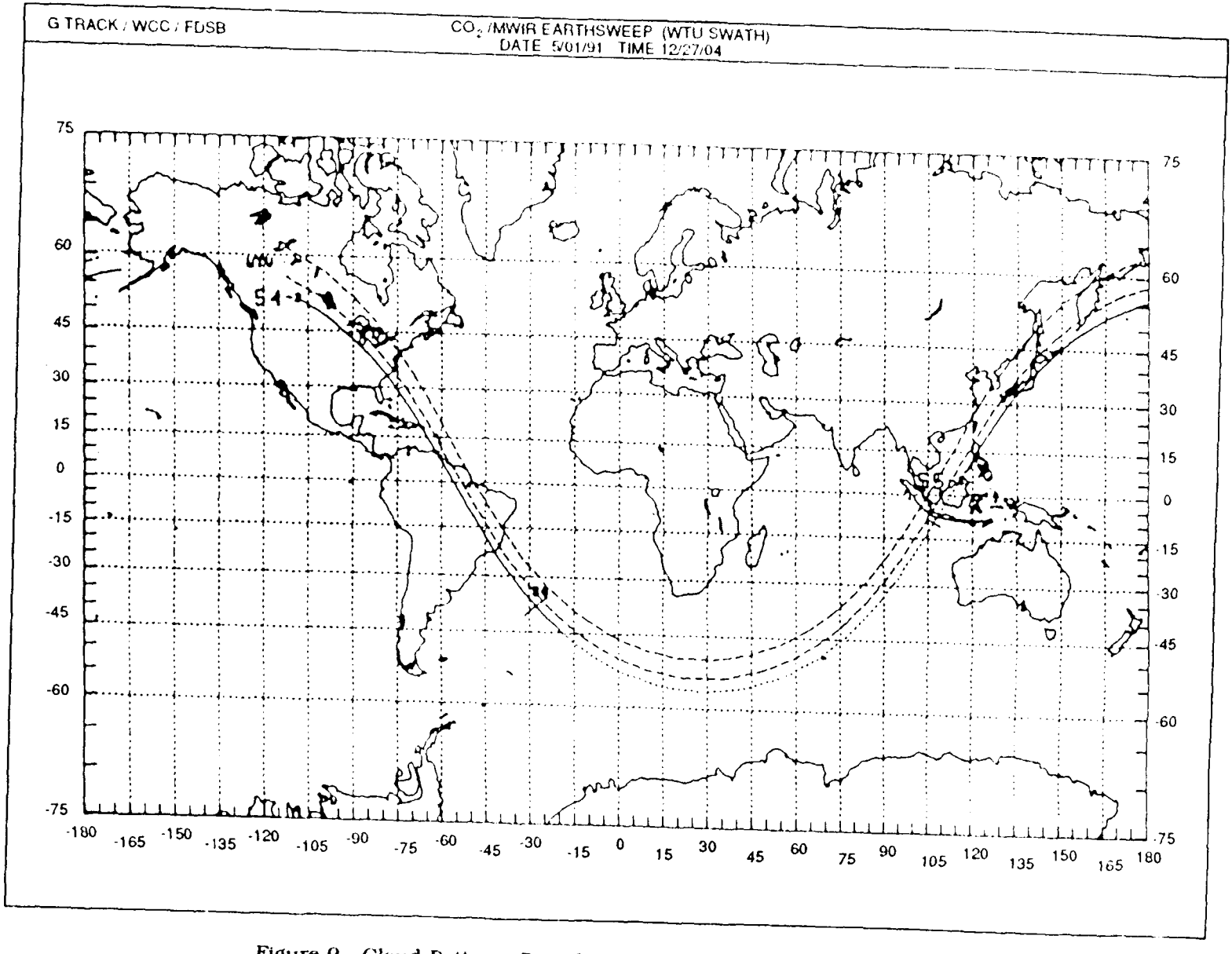


Figure 9. Cloud Patterns Provided by DMSP Imagery.
Provided by Capt. Deanna Ramirez, USAF/Air Weather Service.

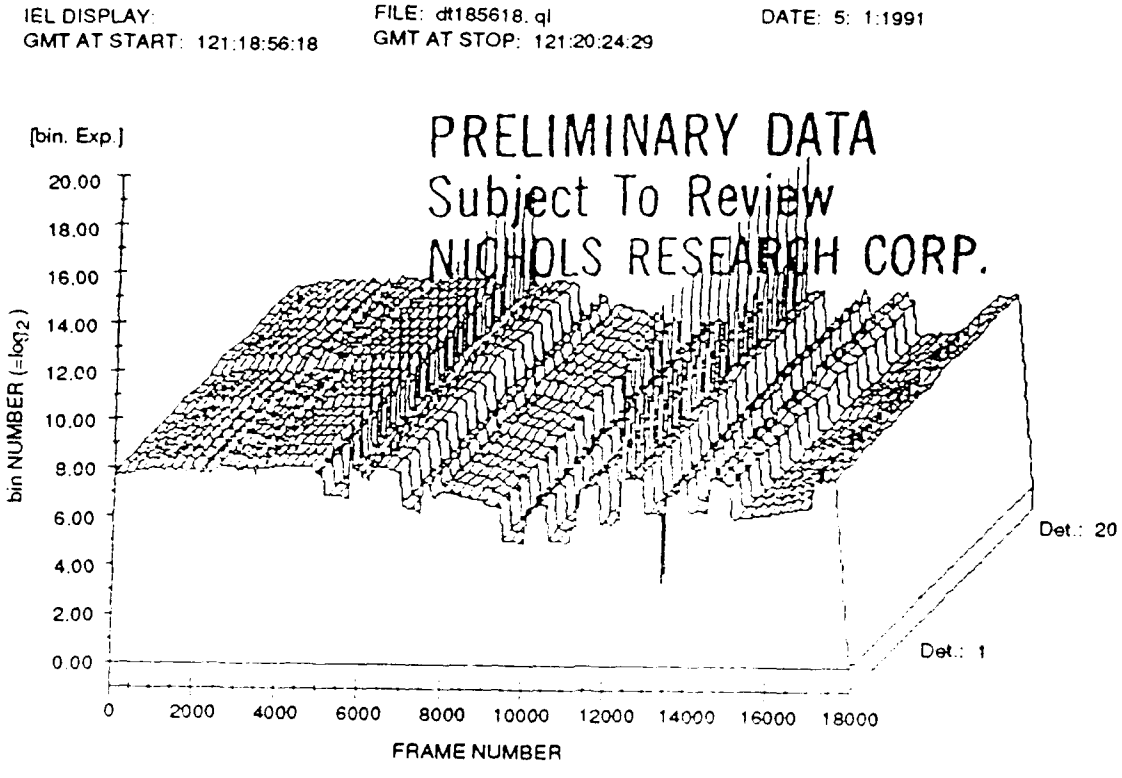


Figure 10. $CO_2$ Earthsweep Data.
Courtesy of Guenter Lange, MBB, GmbH.

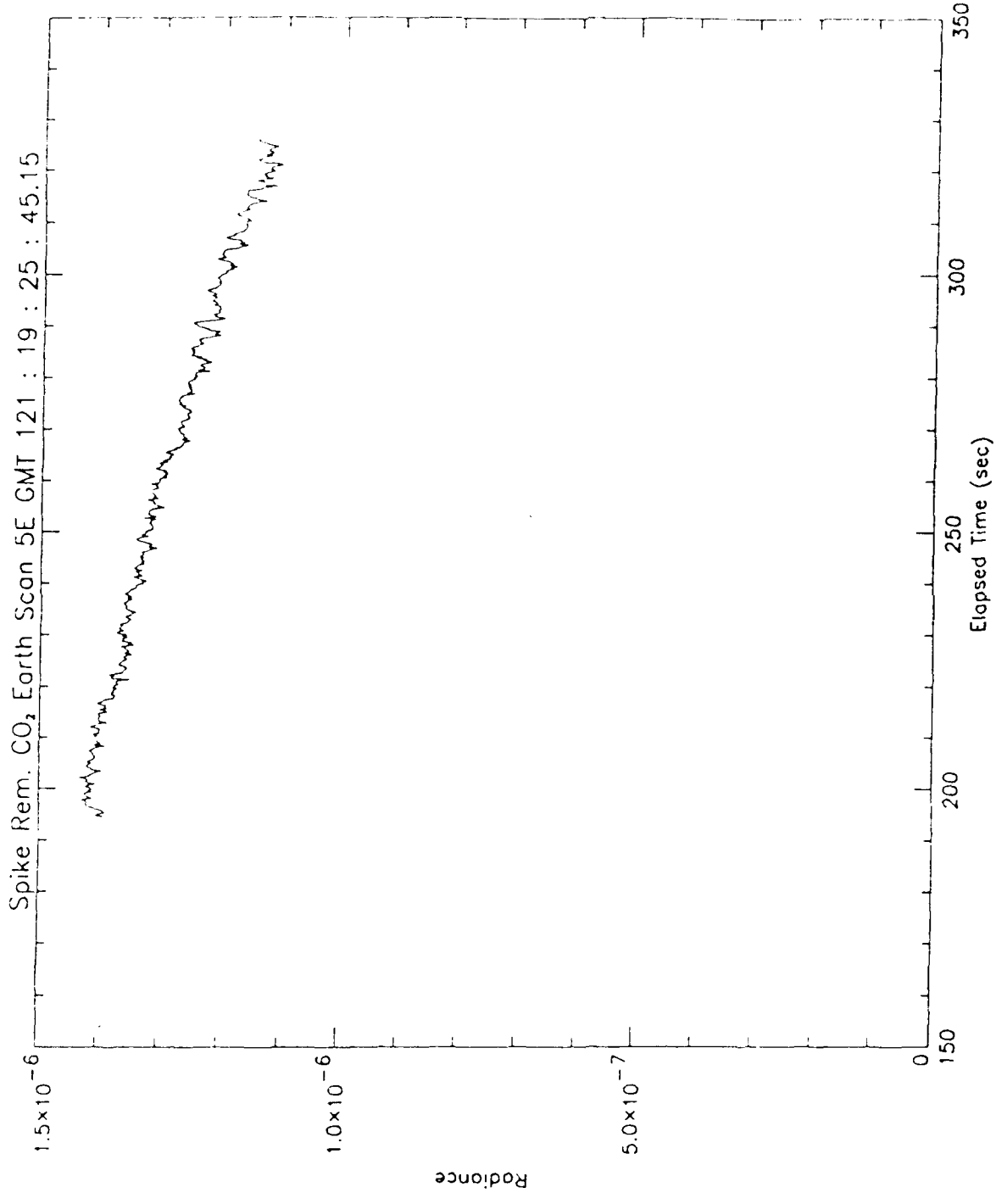


**Figure 11. Example of Narrow-Band $CO_2$ Earthscan Real-Time Data.**

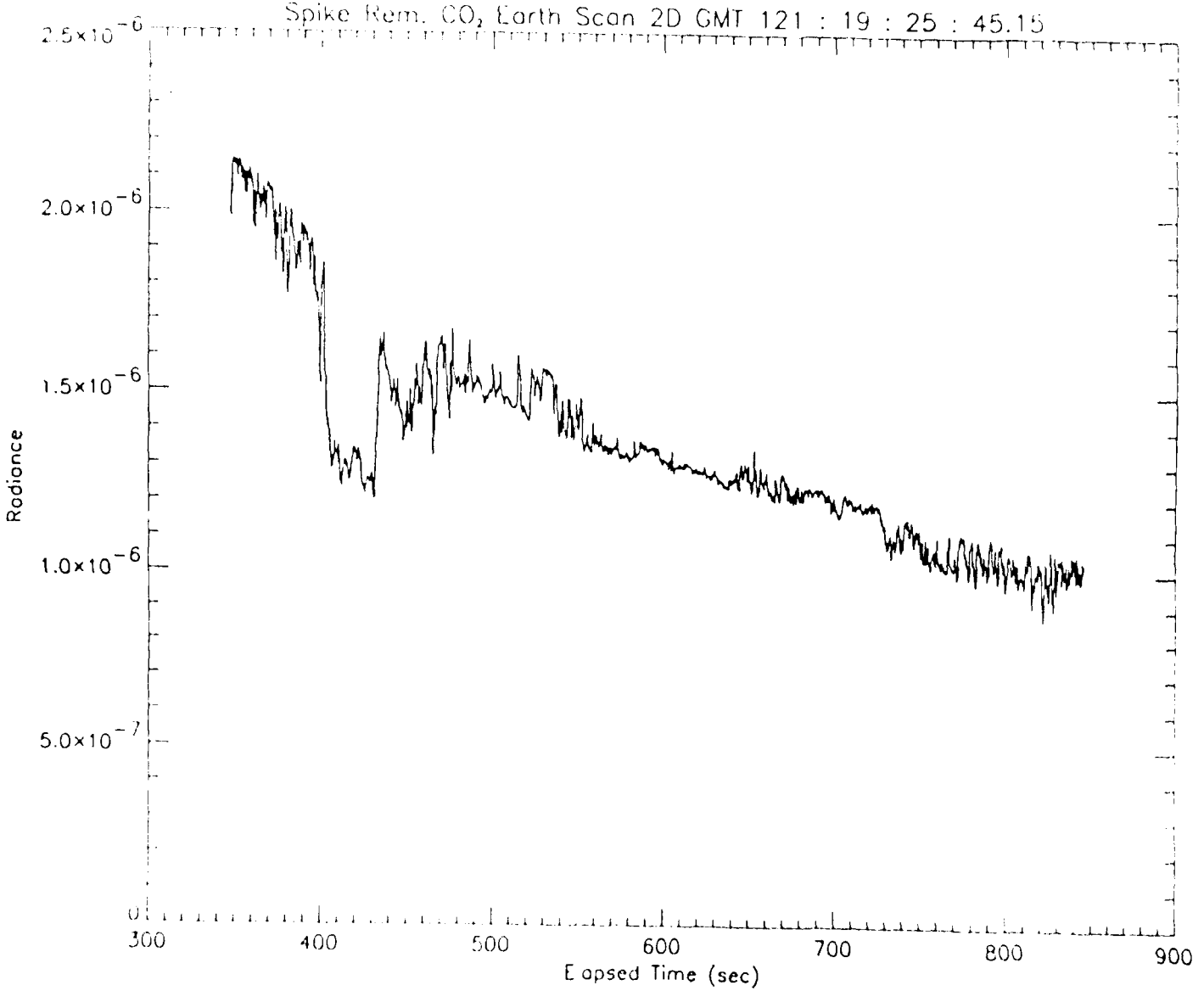


**Figure 12. Example of Wide-Band $CO_2$ Real-Time Data.**

## 4.2 SOLAR SPECULAR POINT

The solar specular point (SSP) measurements in the wide band (filter 2D; bandwidth, 0.25 μm) and narrow band (filter 5E; bandwidth, 0.10 μm) $CO_2$ bands at 4.3 μm were the highest priority objectives of the IBSS backgrounds experiment. The time and location of all the solar specular point observations are shown in Table 8. The first measurement of the SSP was performed during orbit 57 over the Pacific Ocean (see Figure 13) using the wide-band filter 2D. An example of these data is shown in Figure 14. Preliminary review of these data showed unexpected levels of signal fluctuation during this measurement. As a result of this assessment, an additional observation of the SSP in each of the wide and narrow $CO_2$ bands was scheduled. Data is also available from the $L^3TV$ cameras which were on during the observation. Pointing during the experiment was stable with the roll, pitch, and yaw angles of 53.0, -46.6, and 136.12 degrees respectively.

The second SSP observation used filter 5E, the narrow-band $CO_2$ filter. The radiance from this particular band was expected to be spatially uniform, but these data also show unexpected structure. The measurement was made during orbit 80 southwest of Japan as shown in Figure 15. The roll, pitch, yaw angles were 49.69, -43.77, and 139.9 degrees An example of the data is shown in Figure 16.

Table 8. Time and Location of IBSS Solar Specular Point Observations

| SSP# | Start Time-GMT dy:hr:min | End Time-GMT dy:hr:min | Orbit | Location | |
|---|---|---|---|---|---|
| | | | | Latitude | Longitude |
| 1 | 121:23:41 | 121:23:59 | 57 | 15 N | 135 W |
| 2 | 122:04:11 | 122:04:24 | 60 | 5 N | 165 E |
| 3 | 122:15:54 | 122:16:12 | 68 | 18 N | 30 W |
| 4 | 122:20:26 | 122:20:44 | 71 | 30 N | 97 W |
| 5 | 123:15:58 | 123:16:08 | 84 | 25 N | 35 W |
| 6 | 123:20:33 | 123:20:53 | 87 | 5 N | 90 W |

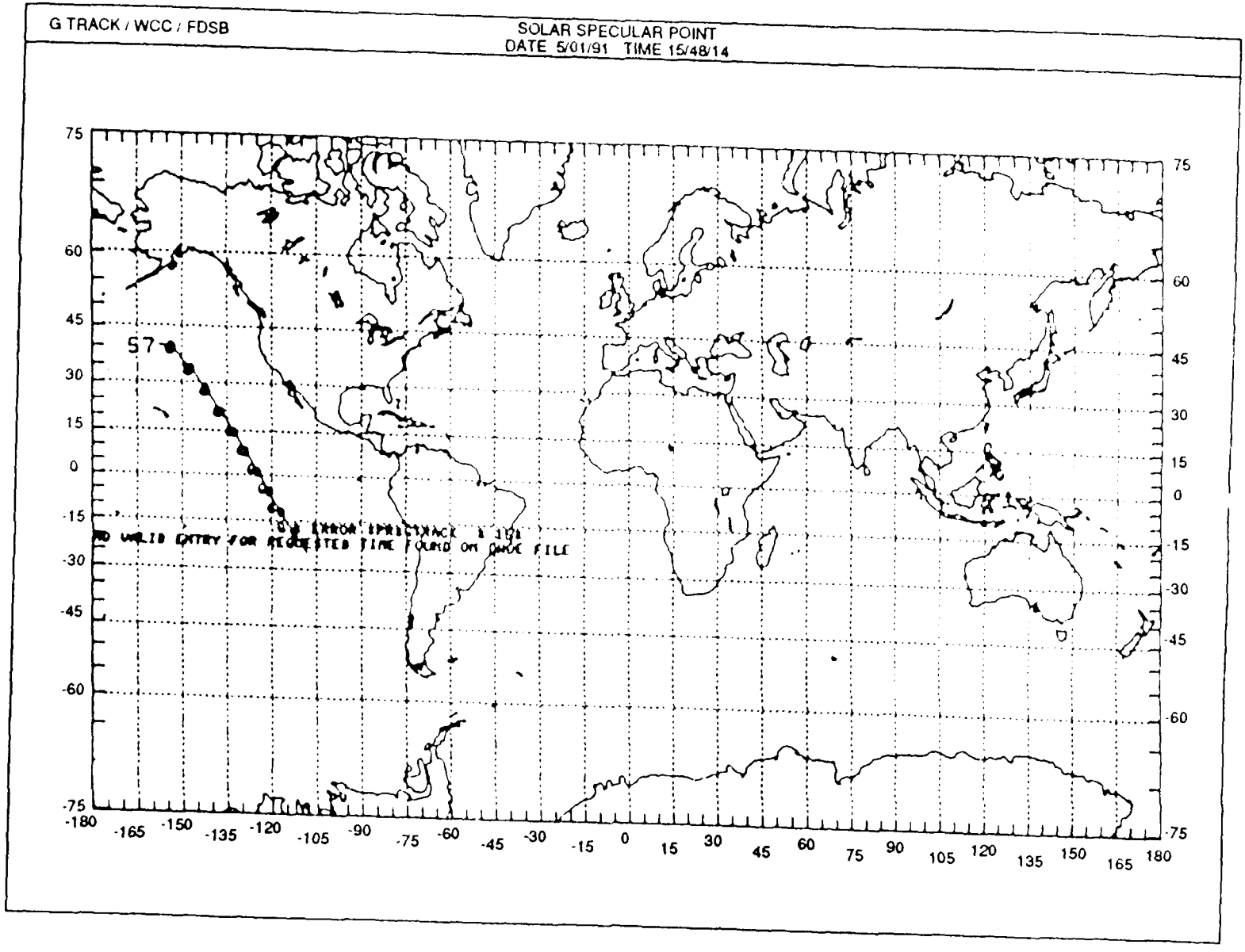


Figure 13. Spacecraft Track for SSP (2D) Measurement.

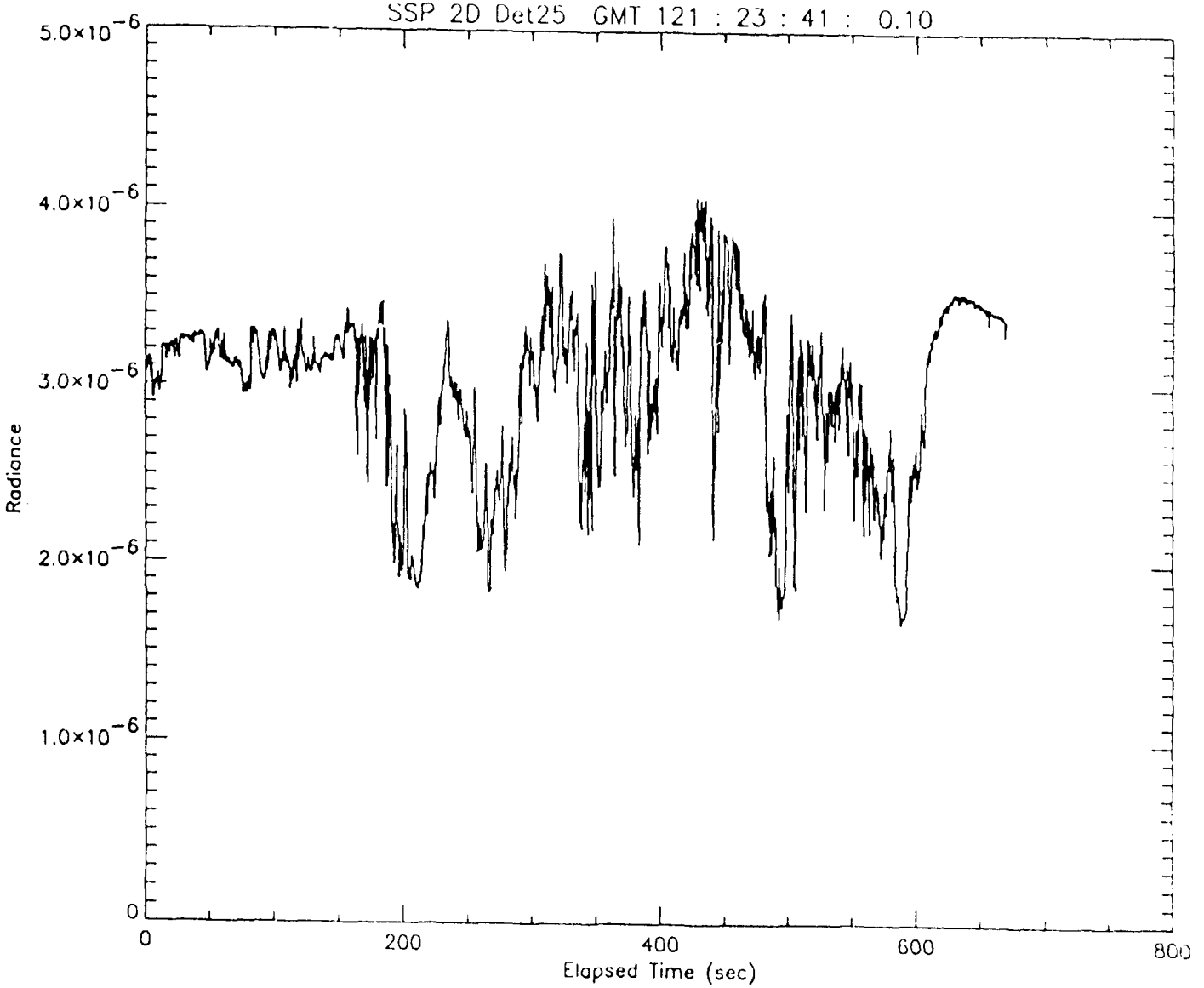


Figure 14. Wide-Band $CO_2$ Solar Specular Data.

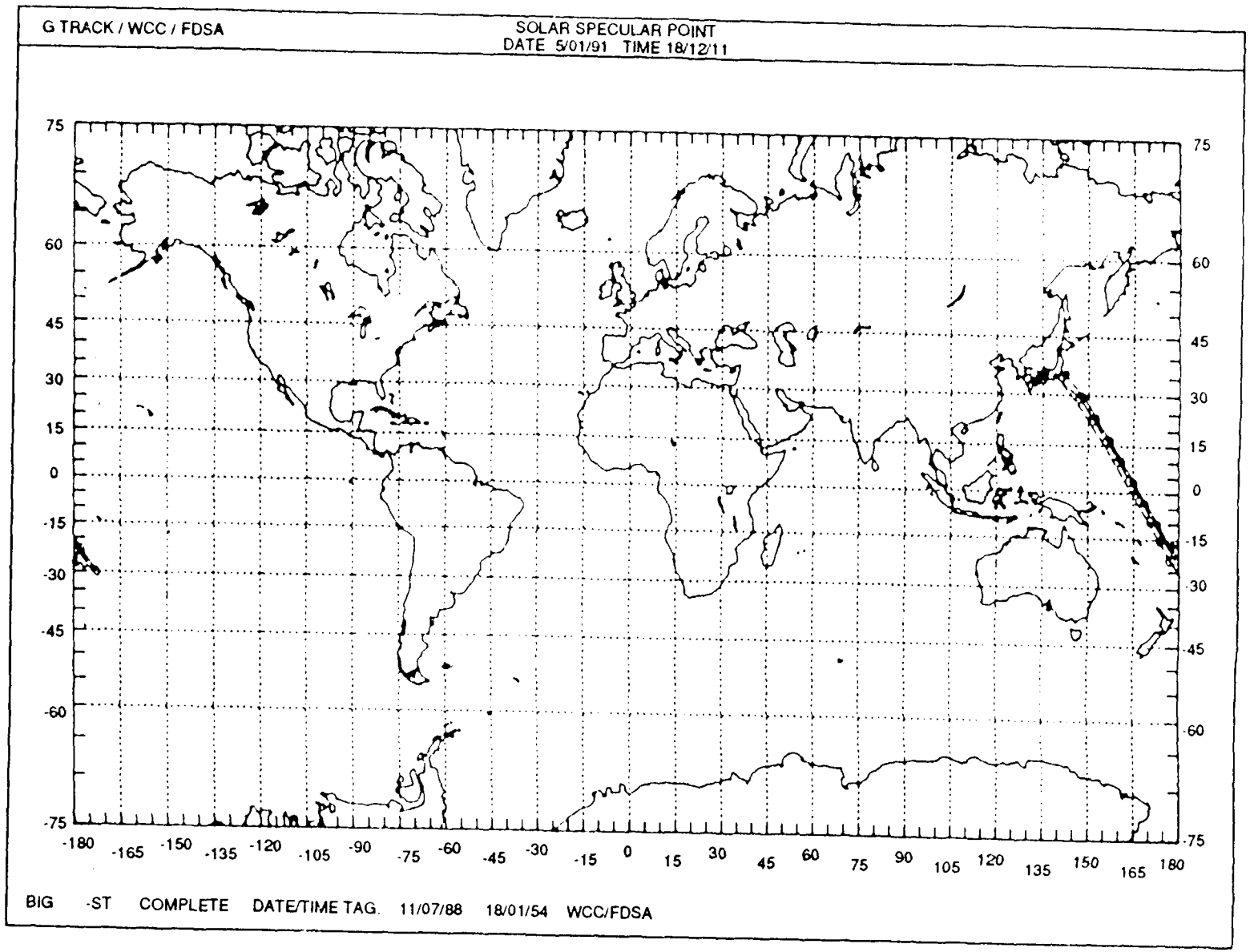


Figure 15. Spacecraft Track for SSP (5E) Measurement.

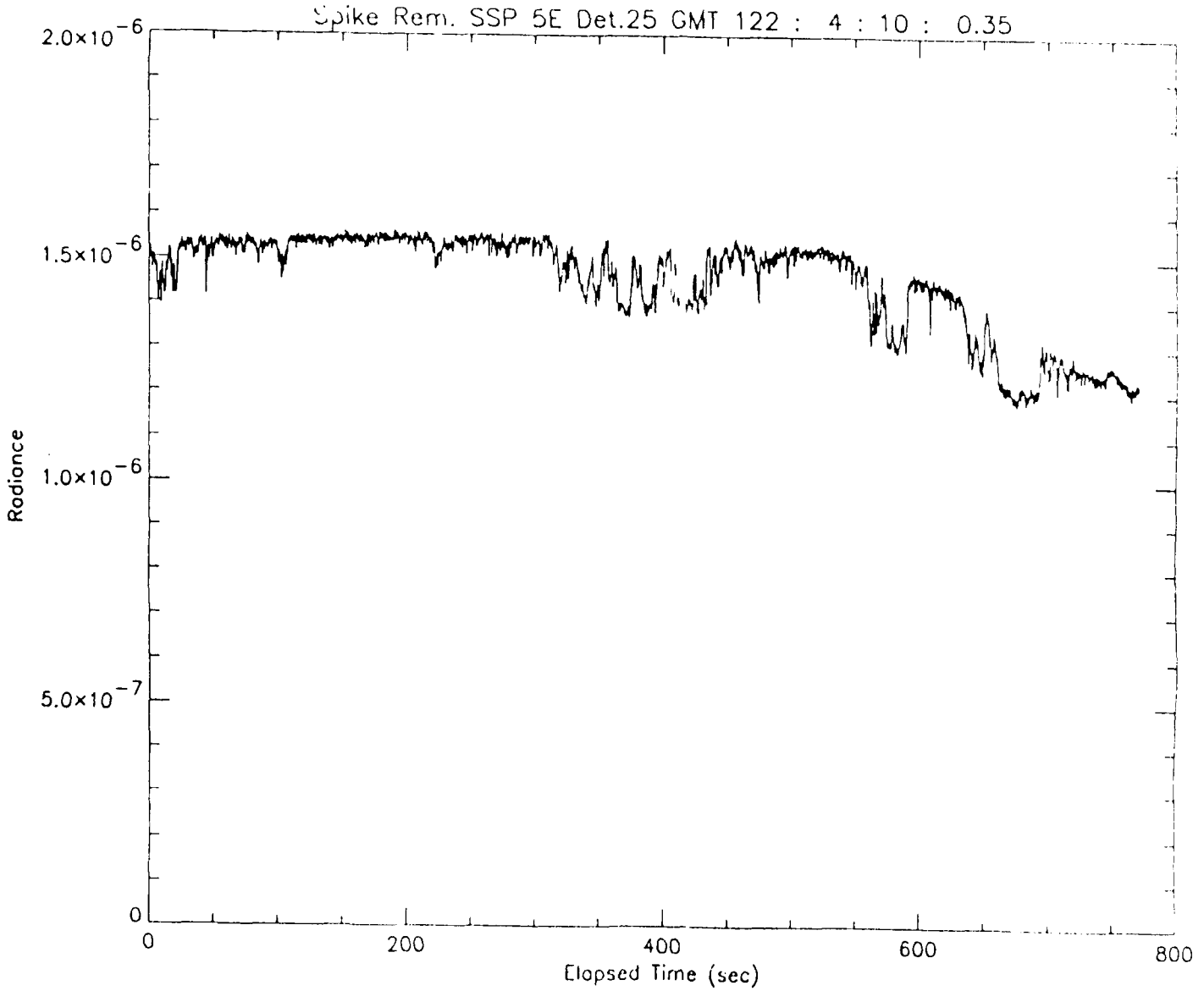


Figure 16. Narrow-Band $CO_2$ Solar Specular Data.

The third measurement of the SSP was a repeat of the narrow-band $CO_2$ measurement. The roll, pitch, and yaw angles were 59.6, -57.3, and 124.88. The observations were over the Atlantic Ocean between Newfoundland and the west coast of Africa. Again, the measurements showed high level signal fluctuations.

The fourth measurement of the SSP was made in the 6.3 μm band using filter number 7C. The roll, pitch, and yaw angles were 66.6, -61.1, and 116.26 degrees. These observations extended from western Canada to the west coast of South America. Figure 17 shows a presentation of these data produced by MBB.

The fifth observation of the SSP was a repeat of filter 2D and was made on the remote manipulator system (RMS). The roll, pitch, and yaw angles were 54.5, -59.7, and 129.7 degrees. These were made over a similar position of the earth as those of previous 5E measurement, extending over the Atlantic Ocean from south of Newfoundland to the western coast of Africa. Figure 18 shows an example of these data.

The final observation of a SSP was a measurement using the IBSS spectrometer. The track ran between the western United States and the western coast of Peru and Ecuador. The roll, pitch, and yaw angles were 47.5, -51.1, and 141.1 degrees.

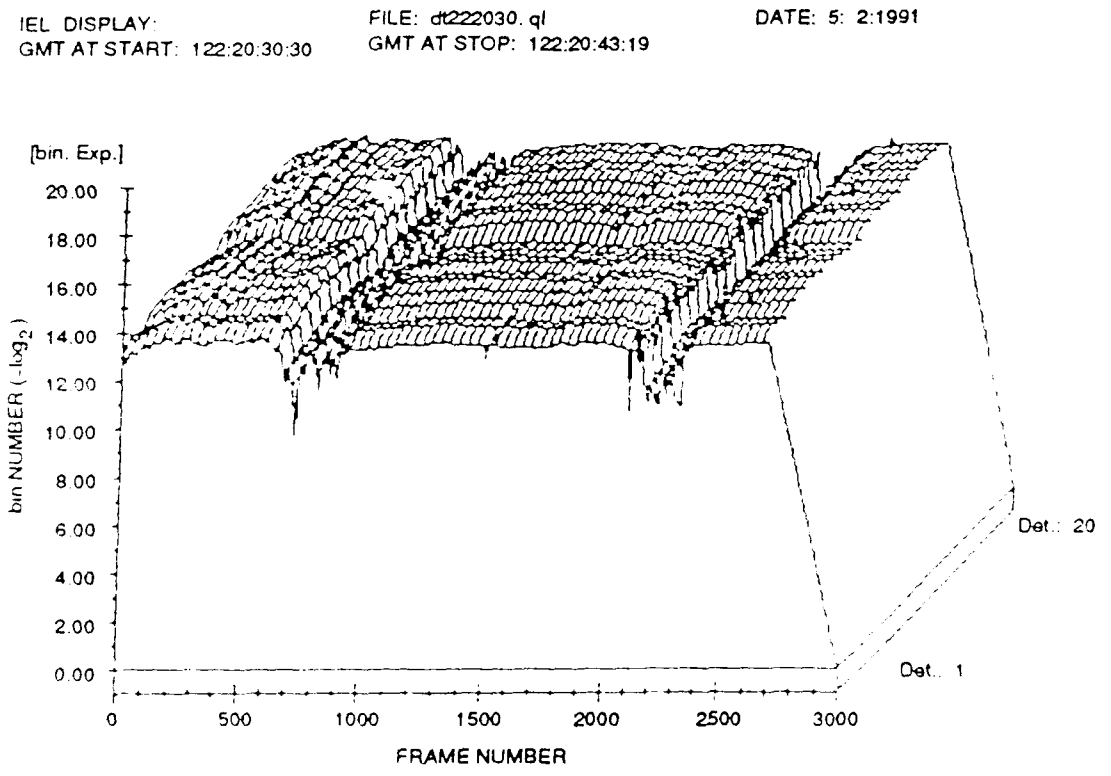


Figure 17. SSP/Spatial Scan Data for 6.3 μm Filter (7C). Courtesy of Guenter Lange, MBB, GmbH.

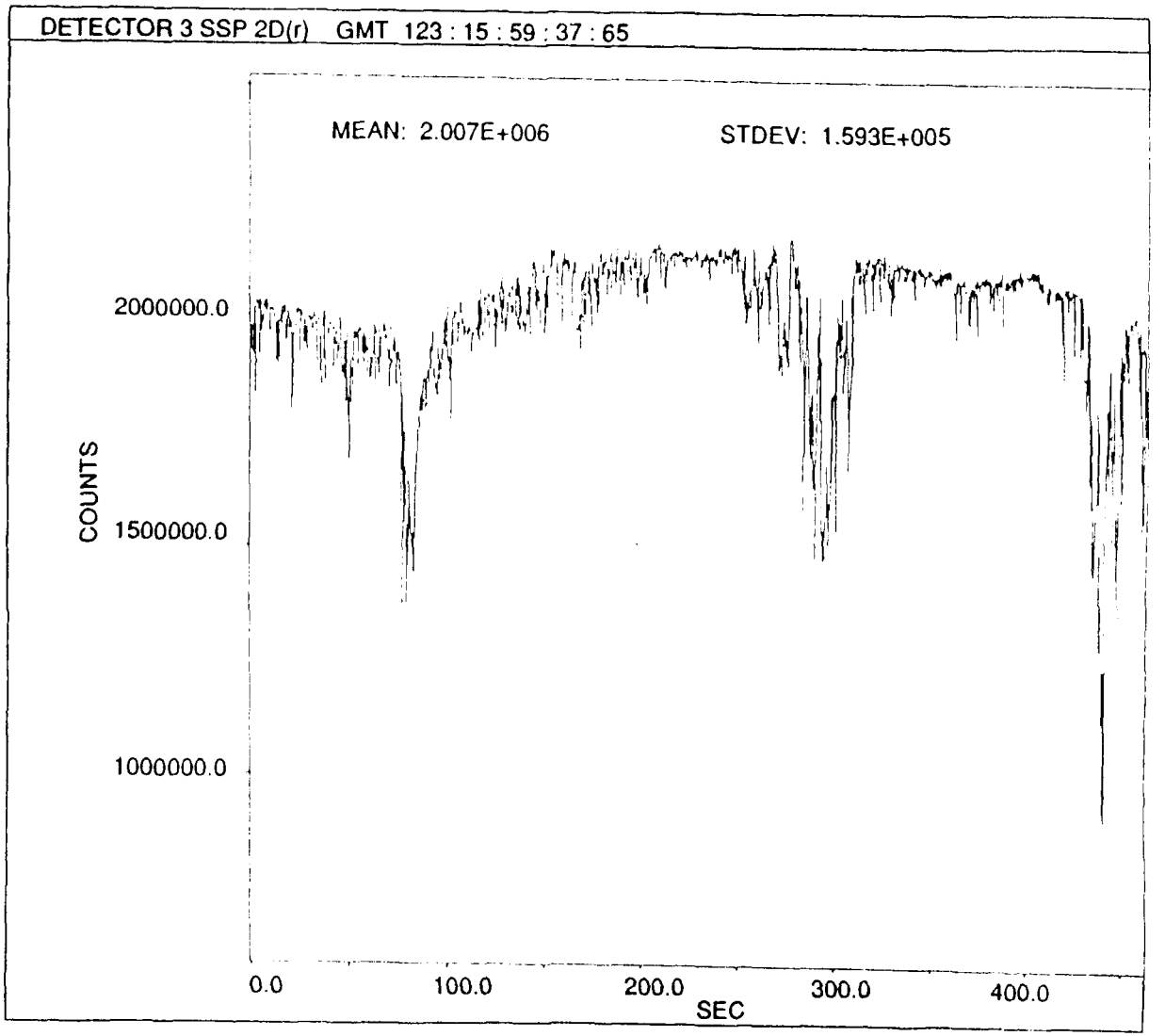


Figure 18. Repeat of Wide-Band Solar Specular Data.

### 4.3 $CO_2$ Earthlimb

The $CO_2$ earthlimb measurements were planned as horizontal limb scans at 30, 45, and 60 km tangent altitudes during day, night, and over the dawn and dusk terminators while alternating between the two $CO_2$ filters. The filter change was controlled by a manual command set. The duration of each of the measurements was 2 minutes. The $CO_2$ earthlimb measurements were taken over a single period that extended over a full orbit. During the pass over the southern auroral zone, the mission specialist reported seeing an aurora to the south. The measurement line of sight was to the north of the orbit, however the orbiter may have been flying through the aurora. The measured Euler angles were close to the planned values, but the actual tangent altitudes viewed will have to be constructed using the SPAS ephemeris and attitude data. Because of the nature of the $CO_2$ profile, the radiance values themselves may contribute to an understanding of the pointing characteristics of the SPAS.

### 4.4 Measurement Set 2

Measurement Set 2 was designed as a series of 30 second horizontal earthlimb scans using all of the filter bands in a pushbroom mode at tangent altitudes of 30, 45, and 60 km, during day and night, and over both terminators. Measurements were made both in the deployed and RMS modes. The roll, pitch, and yaw angles were planned as -90, -14.96, and -100. The actual attitude angles were close to these values, but the actual tangent altitude of the lines of sight will be constructed by using the orbiter ephemeris and the SPAS attitude data.

### 4.5 NO Earthlimb

The NO earthlimb is very similar in operation to Measurement Set 2, but is restricted to higher tangent altitudes where only the radiation from NO is significant. Measurements were made on the RMS at two tangent altitudes. Nominal roll, pitch, and yaw angles were planned as -90.0, -12.99, and -100 (tangent altitude of 100 km) with a pitch change to -12.41 (tangent altitude of 115 km). This measurement suffers from instability and uncertainty in the tangent altitude, which will have to be constructed by using the orbiter ephemeris and the SPAS attitude data.

### 4.6 Limb to Earth Scans

The limb-to-earth scans were designed as a series of vertical scans in either direction between the local horizontal and 5 degrees below the hard earth. The limb-to-earth scans used either a single filter, as indicated in Table 7, or cycled through all the filters in a pre-

programmed sequence. Observing the attitude data in real time indicated that the SPAS was pointing correctly during these scans. Again, the tangent altitude will be constructed by using the SPAS ephemeris and attitude data.

### 4.7 MWIR Earth Scan

The MWIR earthscan was similar in concept to the $CO_2$ backgrounds measurement. It was planned to scan the earth while manually sequencing between the two MWIR filter bands 4D and 7C. The MWIR earthscan was accomplished over several observation blocks as indicated in Table 7. They covered day, night, and two terminators. The initial attitude angles were similar to those of the $CO_2$ backgrounds measurement.

### 4.8 Aurora

While auroral measurements were a high priority for the CIRRIS 1A experiment, these measurements were a relatively low priority for the IBSS experiment. This is because of a fundamental difference in the focus of the two experiments. CIRRIS 1A was designed primarily to investigate high tangent altitudes in the earthlimb in the long-wavelength region of the infrared spectrum (LWIR). IBSS was designed primarily to investigate the short- and mid-wavelength infrared (SWIR and MWIR) primarily while looking down at the hard earth or in the low earthlimb.

The IBSS auroral measurements consisted of scanning the mirror while sequencing the filter wheel through filter numbers 4D, 6C, 2D, and 1C. IBSS measurements were made over the northern auroral region during the daytime. The $L^3TV$ cameras were on during the measurement and are required to provide accurate pointing information. Because the aurora was sunlit, it was not apparent in the $L^3TV$ pictures; therefore, the mission specialist pointed the line of sight at a constant position of approximately 85 km above the hard earth.

# APPENDIX A

## Predicted IBSS Radiances

*by William F. Grieder and Cynthia J. Beeler*

One of the difficult tasks in the IBSS data verification is to confirm the scientific quality and consistency of the measured IR database. The effects of telescope leakage and optical filter leakage must be studied and analyzed to insure these effects did not corrupt the data. Models will be used to predict off-axis and out-of-band radiance, and this will be compared with the off-axis solar experimental data. The effects of contamination, such as particles in the field of view and spikes from high energy particle hits must also be ascertained. The latter is a complex task since the demodulation and averaging of the IBSS signals are accomplished prior to recording so that the effects of spikes are averaged over several data points. In focal plane arrays such as the IBSS sensor a self-consistency check can be accomplished during earthlimb scans that can provide evidence on responsivity stability as well as detector alignments. Measured radiance tangent height profiles will be compared to other validated databases, such as SPIRE, ELIAS, SPIRIT I, and CIRRIS, as well as predictive models, such as SHARC and FASCODE, to establish the quality of the data.

The profiles to be compared with the flight data are called radiance templates. Thus one of the primary preflight tasks was to assemble the databases (and templates) to perform the comparisons. The SHARC earthlimb spectral radiance model provides one of the primary sources of the data required. This model was run at a spectral resolution of 0.5 wavenumbers and then integrated over the IBSS radiometer passbands for both day and night conditions. Figure 3 illustrates the SHARC spectra for both day and night and indicates the positions of

the IBSS filters relative to the spectrum. The SHARC model was run from 60 to 100 km in 1 km steps and the radiance tangent height profiles for each are shown in Figures A1 through A4. These data have been incorporated in verification software where the actual comparisons will take place.

Unfortunately the SHARC predictive code does not yet include the emissions from the hydroxyl (OH) bands, which will be an important source at night within the IBSS filter 2D passband. In this case the SPIRE measurements will be substituted for this template.

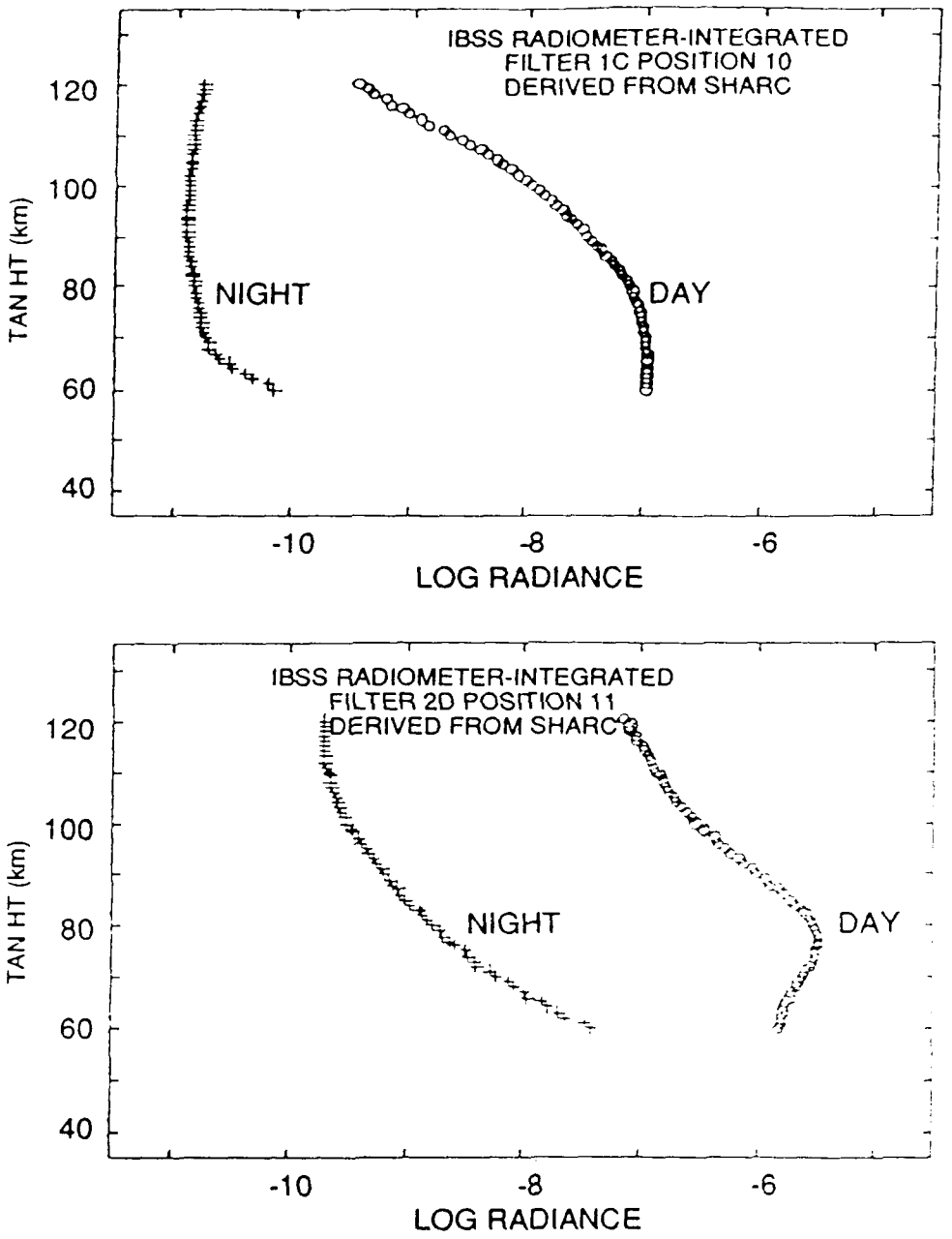


Figure A1. Predicted (SHARC) Inband Radiances for the IBSS Radiometer Filters 1C and 2D Viewing the Earthlimb.

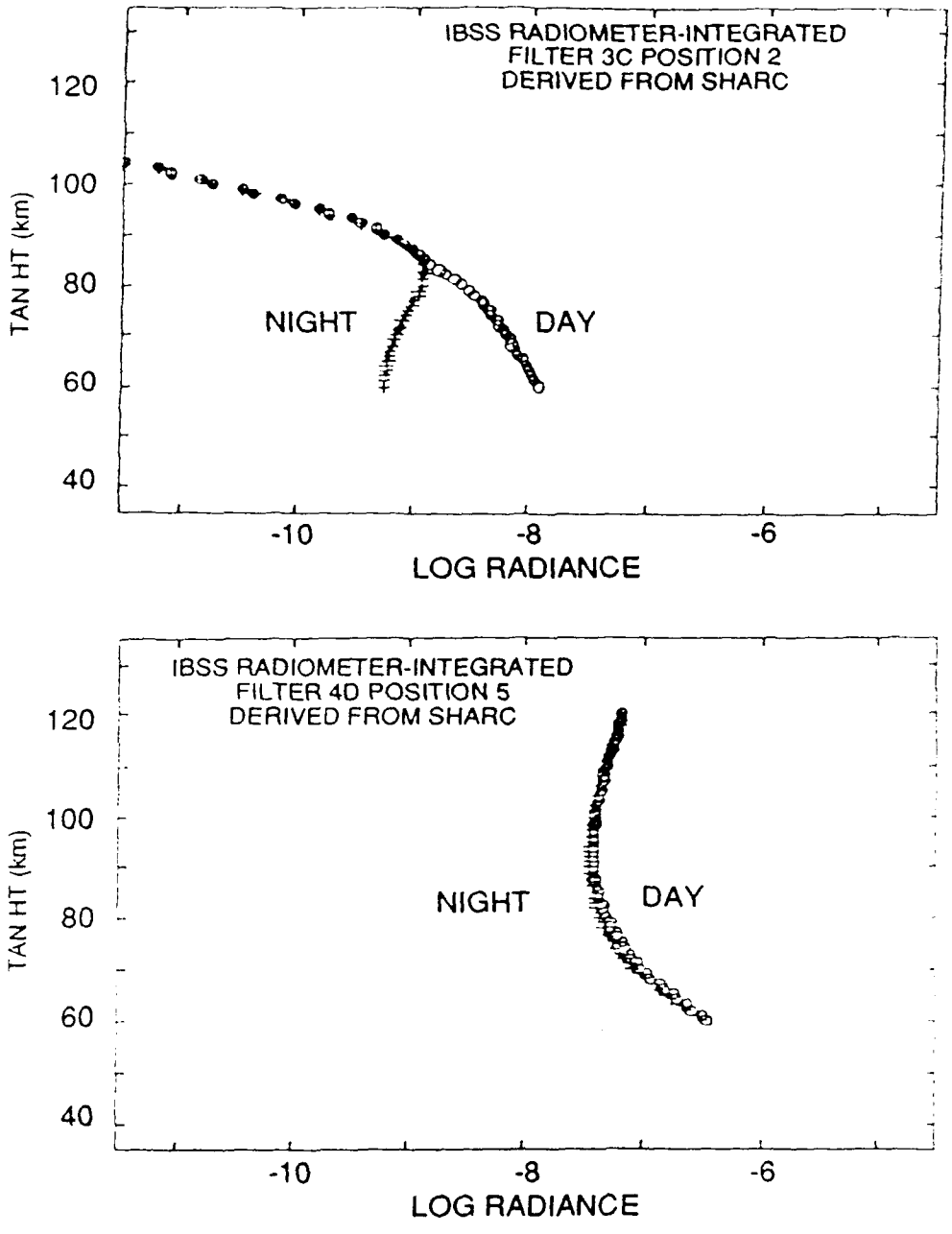


Figure A2. Predicted (SHARC) Inband Radiances for the IBSS Radiometer Filters 3C and 4D Viewing the Earthlimb.

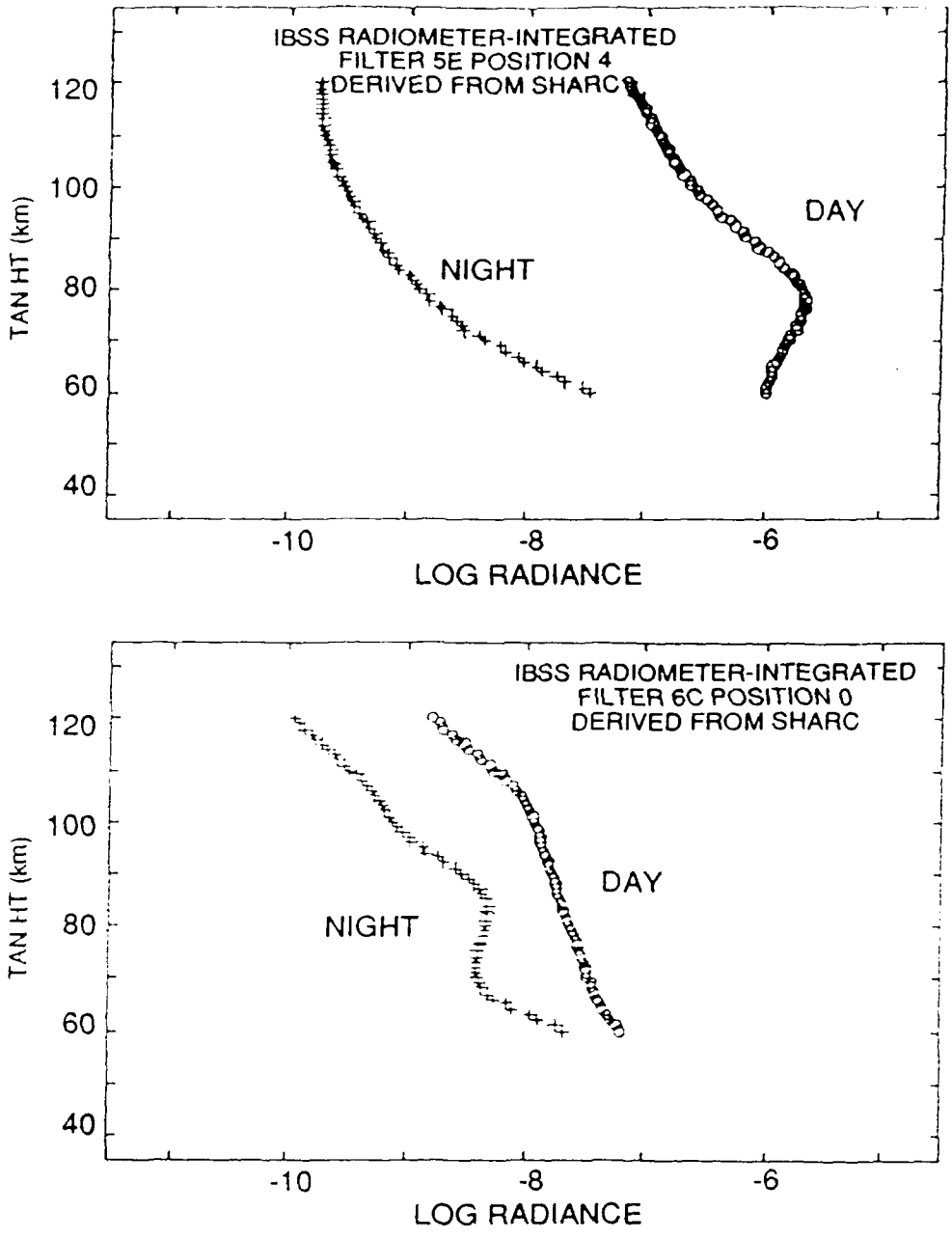


Figure A3. Predicted (SHARC) Inband Radiances for the IBSS Radiometer Filters 5E and 6C Viewing the Earthlimb.

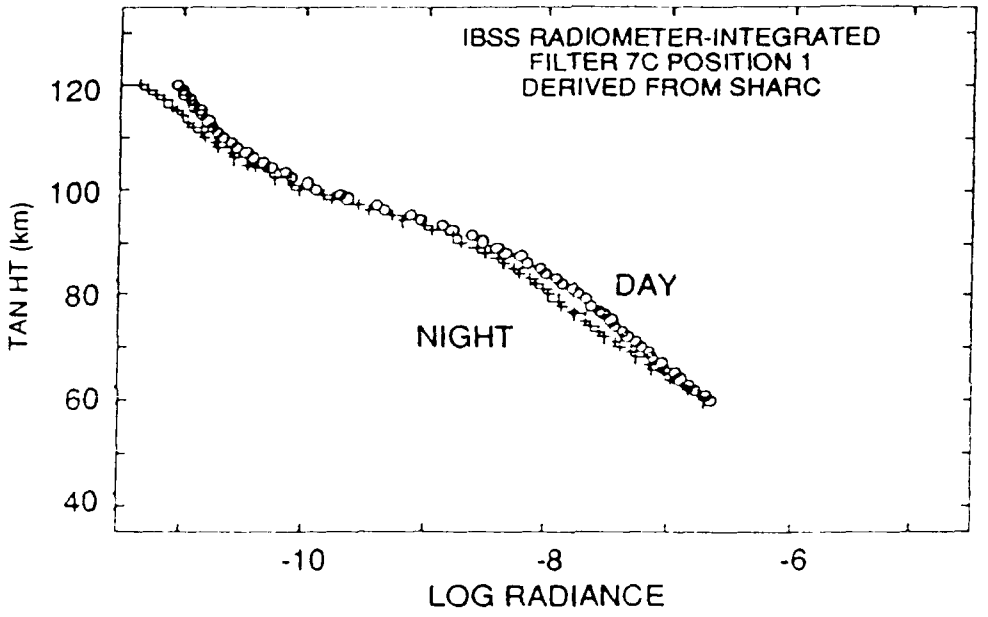


Figure A4. Predicted (SHARC) Inband Radiances for the IBSS Radiometer Filter 7C Viewing the Earthlimb.

# APPENDIX B

## Preliminary SPAS Attitude and LOS Pointing

*by William F. Grieder and Debra S. Autgis*

The SPAS attitude determines the IBSS sensor line-of-sight (LOS) pointing and consequently the tangent height viewed by the focal plane. Spacecraft attitude is described in Euler angles that must have a specific sequence. For SPAS the sequence is yaw, pitch, and roll. The body coordinates for SPAS are such that the x-axis is aligned with the TV camera, the z-axis is down when the x-axis is horizontal, and the y-axis makes a right hand coordinate system, as shown in Figure B1. Body coordinates are given in lower case letters. The transformation from detector angular coordinates to direction cosines, shown in Figure B1, is:

$$\begin{aligned} \cos\alpha x &= \cos az \cos ax \\ \cos\alpha y &= \cos az \sin ax \\ \cos\alpha z &= -\sin az \end{aligned} \qquad \text{(B1)}$$

where

| | | |
|---|---|---|
| $\alpha x, \alpha y, \alpha z$ | = | direction cosines |
| ax | = | detector angular displacement from LOS centerline in the x-direction of object space |
| az | = | detector angular displacement from LOS centerline in the z-direction of object space |

The detector angular displacements (offsets) from the LOS centerline are given in Table B1 (taken from the USU Calibration Report) for the IBSS radiometer. The offsets for the spectrometer are given in Table B2. The detector alignment vector **A** is given as

$$\mathbf{A} = u_x Ax + u_y Ay + u_z Az \qquad \text{(B2)}$$

$$\mathbf{A} = u_x \cos\alpha z + u_y \cos\alpha y + u_z \cos\alpha z \qquad \text{(B3)}$$

where $u_x$ , $u_y$ and $u_z$ are unit vectors.

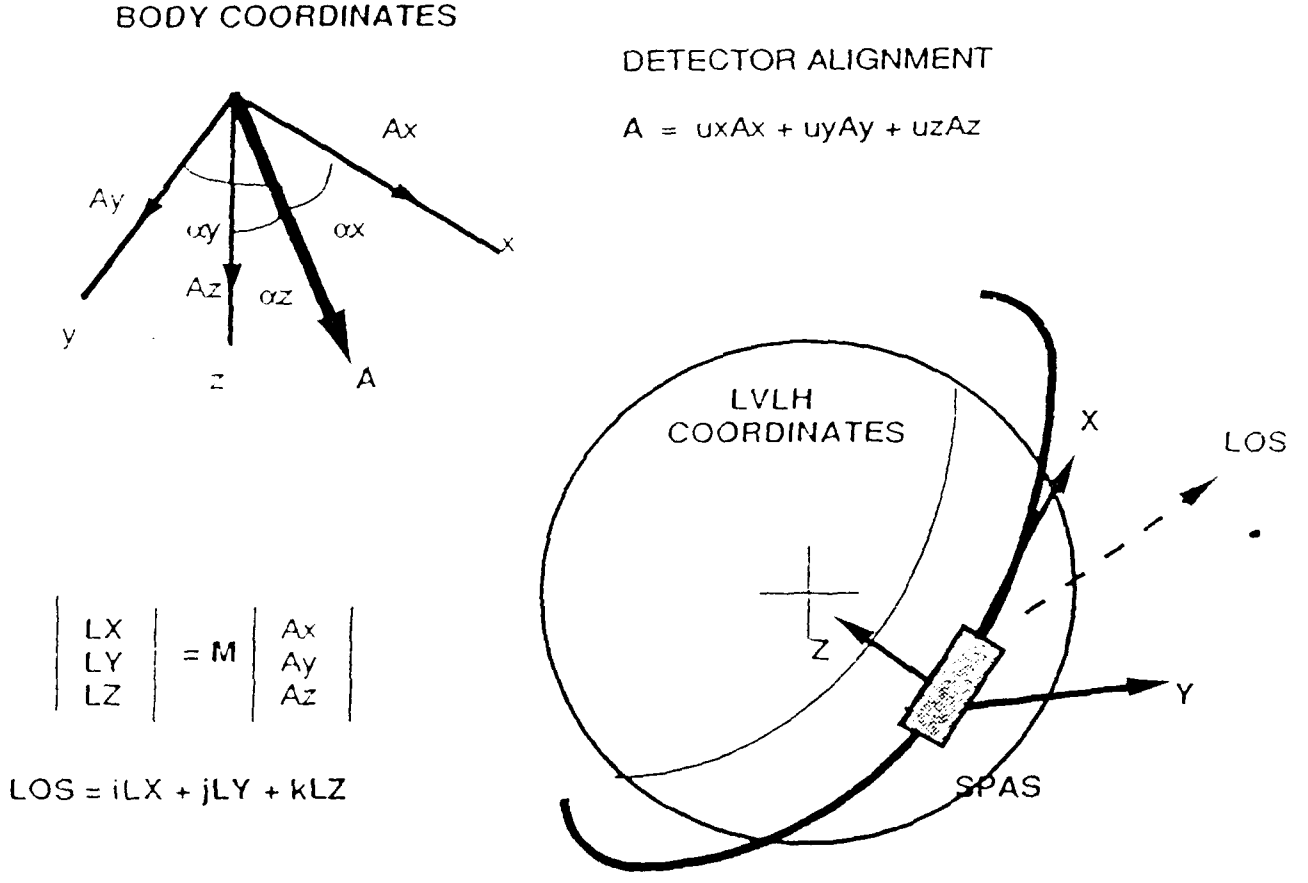


Figure B1. Diagram Showing the Detector Alignment Vector A in Body Coordinates and the Sensor LOS Vector in the LVLH Coordinate System.

## DETECTOR ANGULAR OFFSETS (CENTROID) FROM SPECTROMETER REFERENCE (OBJECT SPACE)

Table B1. IBSS Radiometer Detector Offsets

| angles in milliradians | | | | | |
|---|---|---|---|---|---|
| Detector | ax | az | Detector | ax | az |
| 1 | 11.49 | -7.79 | 2 | 11.49 | -7.23 |
| 3 | 11.49 | -6.67 | 4 | 11.50 | -6.13 |
| 5 | 11.52 | -5.59 | 6 | 11.54 | -5.03 |
| 7 | 11.54 | -4.48 | 8 | 11.54 | -3.91 |
| 9 | 11.55 | -3.33 | 10 | 11.56 | -2.70 |
| 11 | 11.53 | -2.12 | 12 | 11.52 | -1.27 |
| 13 | 11.56 | -0.70 | 14 | 11.56 | -0.13 |
| 15 | 11.54 | 0.42 | 16 | 11.53 | 1.00 |
| 17 | 11.52 | 1.57 | 18 | 11.54 | 2.12 |
| 19 | 11.52 | 2.71 | 20 | 11.52 | 3.33 |
| 21 | 11.52 | 3.89 | 22 | 11.51 | 4.44 |
| 23 | 9.02 | -6.98 | 24 | 9.09 | -4.73 |
| 25 | 9.20 | -2.42 | 26 | 9.82 | -0.53 |
| 27 | 9.81 | 0.15 | 28 | 9.78 | 2.63 |
| 29 | 10.28 | 6.59 | 29 | 10.18 | 6.59 |

Notes: To convert ax to angle from centerline subtract 10.8 milliradian.
To convert az to angle from centerline add 0.99 milliradian.

Table B2. IBSS Spectrometer Detector Offsets

| angles in milliradians | | | | | |
|---|---|---|---|---|---|
| Detector | ax | az | Detector | ax | az |
| 1 | -0.74 | 2.63 | 2 | -0.75 | -6.26 |
| 3 | -0.73 | 2.48 | 4 | -0.76 | -6.50 |
| 5 | -0.73 | 2.74 | 6 | -0.76 | -6.17 |
| 7 | -0.75 | -6.10 | 8 | -0.73 | 2.72 |
| 9 | -0.76 | -6.02 | 10 | -0.72 | 2.80 |
| 11 | -0.73 | -6.50 | 12 | -0.74 | 2.40 |

The recorded SPAS attitude is referenced to the TV centerline. Since the IBSS IR sensor LOS centerline is essentially aligned with the TV camera no further transformations are needed in the body system unless there is a misalignment.

The reference system that will be used in this treatment is called the local vertical local horizontal (LVLH). Its coordinates are specified in upper case letters. In general the X-axis is in the direction of the horizontal component of the spacecraft velocity vector, the Z-axis is in the local nadir direction and the Y-axis is one that completes the right hand rule: X cross Y yields Z. To transform the detector alignment vector **A** to the LVLH coordinate system the following matrix multiplication is required:

$$\begin{vmatrix} LX \\ LY \\ LZ \end{vmatrix} = \mathbf{M} \begin{vmatrix} Ax \\ Ay \\ Az \end{vmatrix}$$

The line of sight vector LOS is then given by,

$$\mathbf{LOS} = iLX + jLY + kLZ. \qquad \text{(B4)}$$

The matrix M for transforming a vector from the body coordinate system to the LVLH system for a yaw, pitch, roll sequence are given by;

$$M = \begin{vmatrix} \cos\theta p \cos\theta y & \sin\theta r \sin\theta p \cos\theta y & \cos\theta r \sin\theta p \cos\theta y \\ & -\cos\theta r \sin\theta y & + \sin\theta r \sin\theta y \\ \cos\theta p \sin\theta y & \sin\theta r \sin\theta p \sin\theta y & \cos\theta r \sin\theta p \sin\theta y \\ & +\cos\theta r \cos\theta y & -\sin\theta r \cos\theta y \\ -\sin\theta p & \sin\theta r \sin\theta p & \cos\theta r \cos\theta p \end{vmatrix}$$

where $\theta y$, $\theta p$ and $\theta r$ are the spacecraft yaw, pitch and roll attitude respectively. Pitch is a rotation about the y-axis measured positive up from the body xy plane (opposite the z-axis), yaw is a rotation about the z-axis and is positive to the right, while roll is a rotation about the x-axis and is positive for right roll.

When the matrix multiplication is carried out the LOS vector components in the LVLH system are:

$$LX = Ax\cos\Theta p\cos\Theta y + Ay[\sin\Theta r\sin\Theta p\cos\Theta y - \cos\Theta r\sin\Theta y] - Az[\cos\Theta r\sin\Theta p\cos\Theta y + \sin\Theta r\sin\Theta y]$$

$$LY = Ax\cos\Theta p\sin\Theta y + Ay[\sin\Theta r\sin\Theta p\sin\Theta y + \cos\Theta r\cos\Theta y] + Az[\cos\Theta r\sin\Theta p\sin\Theta y - \sin\Theta r\cos\Theta y] \quad (B5)$$

$$LZ = -Ax\sin\Theta p + Ay\sin\Theta r\sin\Theta p + Az\cos\Theta r\cos\Theta p$$

where Ax, Ay and Az are the components of the detector alignment vector (direction cosines) and $\Theta y$, $\Theta p$ and $\Theta r$ are the recorded yaw, pitch and roll respectively of the spacecraft.

The elevation angle (from nadir) of the line-of-sight is found by taking the dot product of Eq.(5C) and the unit vector of the LVLH system (k). The result is

$$\cos Gp = LZ = -Ax\sin\Theta p + Ay\sin\Theta r\sin\Theta p + Az\cos\Theta r\cos\Theta p \quad (B6)$$

and substituting the values of the detector alignment vector we get;

$$\cos Gp = -\cos\alpha x\sin\Theta p + \cos\alpha y\sin\Theta r\sin\Theta p - \cos\alpha z\cos\Theta r\cos\Theta p. \quad (B7)$$

The focal plane centerline is oriented along the x axis of the body coordinates and thus for this case ax = ay = az = 0 and therefore the elevation angle of the the LOS centerline Gpo is;

$$\cos Gpo = -\sin\Theta p \quad (B8)$$

$$Gpo = 90° - \Theta p.$$

This shows that the centerline elevation angle from nadir (Gpo) is dependent upon the spacecraft pitch only and is the supplement of the pitch (pitch is measured positive up from the the body xy plane).

The offtrack angle (Ato) of the centerline of the LOS is given by;

$$Ato = \arctan\left(\frac{Ly}{Lx}\right) = \arctan\left(\frac{\cos\Theta p\sin\Theta y}{\cos\Theta p\cos\Theta y}\right) = \Theta y \quad (B9)$$

since Ay = Az = 0 for the LOS centerline. Thus the LOS centerline offtrack angle depends on spacecraft yaw only. To convert offtrack angle to azimuth angle θ measured from True North

$$\theta = \beta + Az. \tag{B10}$$

Beta is the spacecraft heading measured positive clockwise from True North. The spacecraft heading depends upon the orbit inclination I and the spacecraft geocentric latitude Zp. viz:

$$\beta = \arcsin\frac{\cos I}{\cos \angle p}. \tag{B11}$$

At the ascending node the spacecraft is at the equator and the heading is equal to the complement of the orbit inclination. The maximum latitude that the spacecraft can attain is equal to the orbit inclination and thus the spacecraft heading at this point in the orbit is 90° from True North. As the spacecraft continues toward the descending node the value of Eq.(B11) must be subtracted from 180°.

## TANGENT HEIGHT COMPUTATIONS

The derivation of tangent height requires knowledge of the spacecraft ephemeris and the sensor line-of-sight (LOS) pointing angles for a specific detector. Since the SPAS attitude is referenced to the TV camera and the IBSS IR sensor is aligned with the camera, the recorded yaw, pitch and roll of the SPAS is also that for the IBSS IR sensor. Using the attitude data and the techniques described in this Appendix, the IBSS LOS pointing angles were derived. These angles are defined as the elevation angle (Gp) from nadir and the offtrack angles(At). The geocentric tangent height Ht(D) for any detector D is

$$Ht(D) = A \sin[Gp(D)] - Rt$$

where

A = Rp + Hp
Rp = earth radius at the SPAS position
Hp = SPAS geocentric altitude
Gp(D) = nadir LOS elevation angle for detector D
Rt = earth radius at tangent point.

If the SPAS orbit was perfectly circular then A is the semimajor axis. In this case A was computed from the ephemeris data.

Computing the earth radius at the tangent point is a little more complicated. First the geocentric latitude (Zt) of the tangent point must be found. This is done from the following equation:

$$\sin Zt = \sin Zp \sin Gp + \cos Zp \cos Gp \cos Az$$

where

Zp = geocentric latitude of the SPAS
Gp(D) = defined above
θ = LOS azimuth pointing angle from True North.

The LOS azimuth angle θ is found from the offtrack azimuth angle At and knowledge of the spacecraft heading β , viz:

$$\theta = \beta + At.$$

All angles are measured positive clockwise.

The earth radius Rt at this latitude Zt is

$$Rt = \frac{Re}{\sqrt{\cos^2 Zt + f^2 \sin^2 Zt}}$$

where

Re = earth equatorial radius = 6378.116 km
f = flattening factor Re/Rn = 1.00346.